

AGU Advances



RESEARCH ARTICLE

10.1029/2023AV001121

Peer Review The peer review history for this article is available as a PDF in the Supporting Information.

Key Points:

- Warm conditions in dynamic subduction models promote slab dehydration leading to long-lasting water storage in the upper mantle
- Dynamic thermal-petrologic models show maximum mantle wedge hydration during intermediate stages as the slab sinks through the upper mantle
- Conditions are too warm to stabilize hydrous minerals during subduction infancy and dehydration occurs too deep during mature subduction

Supporting Information:

Supporting Information may be found in the online version of this article.

Correspondence to:

G. S. Epstein, gepstein@uw.edu

Citation:

Epstein, G. S., Condit, C. B., Stoner, R. K., Holt, A. F., & Guevara, V. E. (2024). Evolving subduction zone thermal structure drives extensive forearc mantle wedge hydration. *AGU Advances*, *5*, e2023AV001121. https://doi.org/10.1029/2033AV001121

Received 6 NOV 2023 Accepted 31 MAY 2024

Author Contributions:

Conceptualization: G. S. Epstein,
C. B. Condit, A. F. Holt, V. E. Guevara
Formal analysis: G. S. Epstein
Funding acquisition: C. B. Condit,
A. F. Holt, V. E. Guevara
Investigation: G. S. Epstein, C. B. Condit,
R. K. Stoner, A. F. Holt, V. E. Guevara
Methodology: G. S. Epstein, C. B. Condit,
R. K. Stoner, A. F. Holt, V. E. Guevara
Resources: C. B. Condit, A. F. Holt,
V. E. Guevara

 $\ \ \, \mathbb{O}$ 2024. The Authors.

A. F. Holt

This is an open access article under the terms of the Creative Commons
Attribution License, which permits use, distribution and reproduction in any medium, provided the original work is properly cited.

Evolving Subduction Zone Thermal Structure Drives Extensive Forearc Mantle Wedge Hydration

G. S. Epstein^{1,2}, C. B. Condit¹, R. K. Stoner², A. F. Holt², and V. E. Guevara³

¹Department of Earth and Space Sciences, University of Washington, Seattle, WA, USA, ²Rosenstiel School of Marine, Atmospheric, and Earth Science, University of Miami, Miami, FL, USA, ³Geology Department, Amherst College, Amherst, MA, USA

Abstract Hydration of the subduction zone forearc mantle wedge influences the downdip distribution of seismicity, the availability of fluids for arc magmatism, and Earth's long term water cycle. Reconstructions of present-day subduction zone thermal structures using time-invariant geodynamic models indicate relatively minor hydration, in contrast to many geophysical and geologic observations. We pair a dynamic, time-evolving thermal model of subduction with phase equilibria modeling to investigate how variations in slab and forearc temperatures from subduction infancy through to maturity contribute to mantle wedge hydration. We find that thermal state during the intermediate period of subduction, as the slab freely descends through the upper mantle, promotes extensive forearc wedge hydration. In contrast, during early subduction the forearc is too hot to stabilize hydrous minerals in the mantle wedge, while during mature subduction, slab dehydration dominantly occurs beyond forearc depths. In our models, maximum wedge hydration during the intermediate phase is 60%– 70% and falls to 20%-40% as quasi-steady state conditions are approached during maturity. Comparison to global forearc H₂O capacities reveals that consideration of thermal evolution leads to an order of magnitude increase in estimates for current extents of wedge hydration and provides better agreement with geophysical observations. This suggests that hydration of the forearc mantle wedge represents a potential vast reservoir of H_2O , on the order of 3.4–5.9 \times 10²¹ g globally. These results provide novel insights into the subduction zone water cycle, new constraints on the mantle wedge as a fluid reservoir and are useful to better understand geologic processes at plate margins.

Plain Language Summary Subduction is the process by which old, water-rich rocks of the ocean floor are recycled into the Earth's mantle in a conveyor belt-like system. As this material (the subducting slab) enters the mantle it undergoes heating, releasing its bound water while simultaneously cooling the surrounding mantle. The rate and magnitude of this heating is not constant through time but undergoes a dramatic change over the lifecycle of a subduction zone. Water release during subduction controls where earthquakes and volcanoes do or do not occur and has an impact on cycling between the earth, atmosphere, and oceans. In this study we model the time-varying nature of water storage within the relatively cool uppermost mantle directly above the slab (the forearc mantle wedge). We find that, worldwide, the forearc mantle wedge contains ~1 order of magnitude more water than previously thought, representing a mass equivalent to ~0.4% of Earth's oceans. Temperature changes within the slab and mantle through time are the main cause of this increased hydration. These results are supported by seismic observations and provide insights into the maximum depth of damaging earthquakes, the fluid source for explosive volcanic eruptions, and the dynamic parameters that allow for subduction to progress.

1. Introduction

The subduction zone forearc mantle wedge, coined as the "magic zone" by Marsh (1979), exerts a critical influence on the geodynamics, geochemistry, and geohazards of subduction zones. Hydration of the forearc mantle wedge is thought to impact the distribution and/or downdip limit of seismicity (Oleskevich et al., 1999; Peacock & Hyndman, 1999; Seno, 2005; K. Wang et al., 2020), contribute to the source(s) of melting for arc magmatism (Chen et al., 2021; Hattori & Guillot, 2003; Lee, 2005; Till et al., 2012), and act as a volatile reservoir for subsequent magmatic and tectonic processes (e.g., ignimbrite flare-ups: Farmer et al., 2008; strike slip fault movement: Kirby et al., 2014). The extent of wedge hydration is predicated on fluid availability and on the capacity of the forearc mantle for retaining H_2O , two factors that are dependent on subduction zone thermal structure (Hyndman & Peacock, 2003; Peacock, 1996). Thus, covariations in slab and wedge temperatures over

EPSTEIN ET AL. 1 of 27

Supervision: C. B. Condit, A. F. Holt Validation: G. S. Epstein, R. K. Stoner Visualization: G. S. Epstein

the lifetime of a subduction zone (as are inferred from modeling and observations) will lead to drastic temporal variations in H_2O content of the mantle wedge. Such temporal variability in subduction zone thermal structure has not been accounted for in many previous models of slab dehydration and forearc hydration (e.g., Abers et al., 2017; Hacker, 2008; van Keken et al., 2011).

In the forearc, dehydration reactions within subducting metasedimentary and metamafic rocks release aqueous fluids which are inferred to percolate upward or sub-vertically when permeability is high and buoyancy forces dominate with respect to local pressure gradients (Connolly, 2005; Wilson et al., 2014). Forearc wedge hydration occurs where these fluids infiltrate the nose of the mantle wedge at pressure-temperature (P-T) conditions where hydrous minerals are stable in peridotite (Fyfe & McBirney, 1975; Hyndman & Peacock, 2003). The mineralogy within this zone is dependent on the mantle wedge bulk composition, P-T conditions, and the availability of aqueous fluid to induce hydration (Bromiley & Pawley, 2003; Ulmer & Trommsdorff, 1995). Serpentine group minerals, containing up to 13 wt.% H_2O , are the most volumetrically significant hydrous minerals in the mantle wedge.

Some workers have proposed that modern day thermal conditions of subduction zone forearcs do not lead to large-scale hydration except at very warm margins (e.g., Cascadia: Abers et al., 2017; van Keken et al., 2011). However, geophysical observations (seismic, magnetic, gravity, and heatflow) suggestive of mantle wedge hydration have been noted globally, even along relatively cool margins (e.g., Marianas: Tibi et al., 2008). Hence, while the present-day thermal structure of these subduction zones is unlikely to facilitate wedge hydration, the earlier thermal evolution of these subduction zone forearcs may be vital in stabilizing a persistent serpentinized, or otherwise hydrated, forearc mantle.

Time evolving and dynamic (i.e., without externally imposed forces) numerical models of subduction zone thermal structure may help to resolve this paradox. Such models, which do not impose plate velocities, plate forces, or fix the geometry of the subduction zone, demonstrate substantial time-dependent variation in forearc thermal structure, from soon after subduction initiation through to "steady state" (i.e., time invariant) conditions, after which there is minimal variation (e.g., Holt & Condit, 2021; Zhou & Wada, 2021). Herein we adopt such a modeling approach to explore the evolution of the hydration state of the forearc mantle wedge beginning soon after subduction initiation until quasi-steady state conditions. During the early-to-intermediate stages of subduction—that is, before near steady conditions—our models predict extensive hydration of the mantle wedge, as the slab undergoes dehydration at forearc depths concurrently with cool enough conditions in the wedge for the stability of hydrous phases. We place our modeling results into the context of previously published subduction zone thermal models to compare to evidence obtained from geophysical and petrologic investigations. Our analysis supports the hypothesis that pervasive wedge hydration is a common feature of subduction. See Figure 1 for a cartoon illustration of the model setup, processes, and terminology discussed in this paper.

2. Background

2.1. Geodynamic Models of Subduction Zone Thermal Structure

We broadly distinguish two types of subduction zone thermal models in the present work: kinematically driven and dynamic. In kinematically driven models, thermal fields are generated while holding certain geometrical and kinematic parameters of the subduction zone constant. Such models are typically run until steady-state slab and mantle wedge temperatures are obtained or, for young subduction zones, until thermal conditions match observables (e.g., Nankai margin of Syracuse et al., 2010). Thermal structures obtained from such models are readily applicable to individual, currently active Earth subduction zones, and have thus led to important insights into the mechanisms behind variability in surface heat flow (Gao & Wang, 2014; Wada & Wang, 2009), locations of arcs (England et al., 2004; Syracuse & Abers, 2006), geochemical proxies for slab temperatures (Ce/H₂O; Plank et al., 2009), and sources of volatiles (Epstein et al., 2021; Gorman et al., 2006). However, such models cannot encapsulate the evolution of subduction zones through geological time, where subduction velocities and geometries co-evolve and, in turn, produce co-dependent changes in slab and wedge thermal structure.

The dynamic and time-dependent models considered here do not impose convergence, trench migration, and slab sinking rates. Instead, these parameters evolve freely through time while satisfying an evolving subduction zone force balance. This results in pronounced variability in convergence rate and slab dip, which, in turn, manifests in

EPSTEIN ET AL. 2 of 27

subducting plate/slab

upper mantle

ower mantle

hydrated

crustal

section (Fig. 3)

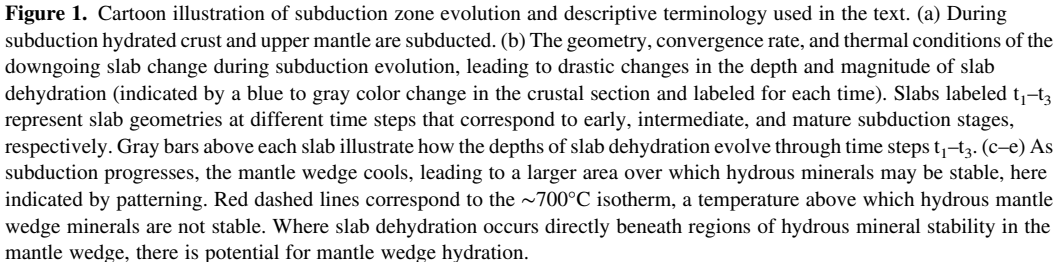


overriding plate

slah

depth

ydrous minerals stable in mantle wedge dehydration



highly time dependent slab *P-T* conditions (Holt & Condit, 2021; Kincaid & Sacks, 1997; Zhou & Wada, 2021). We note that time dependent subduction zone thermal structure can also be modeled using a kinematically driven approach, by either varying imposed subduction properties like convergence rate or plate age (e.g., Peacock & Wang, 1999; Suenaga et al., 2019; K. Wang et al., 1995) or by examining the transient phase in models that impose constant subduction properties yet retain time dependence in the thermal (energy) solution (e.g., Hall, 2012). However, because these hybrid approaches impose slab properties, they are unable to investigate the time-dependence of subduction zone thermal structure within a framework that permits the slab and mantle wedge to co-evolve in a dynamically consistent manner.

As an example, in kinematically-driven thermal models, the decoupling depth (DD; below which the slabtop and overlying mantle wedge are coupled) is typically set at a constant depth of 80 km. This imposes the depth at which the convective mantle wedge can induce rapid slabtop heating (e.g., the "D80" model of Syracuse et al., 2010), thereby exerting a strong control on the temperature profile and bounding dehydration to depths greater than 80 km (except in select cases: e.g., Cascadia; van Keken et al., 2011). The DD is unlikely to be constant over time (Holt & Condit, 2021; Kerswell et al., 2021; Y. Wang et al., 2023). Incorporating a variable DD in dynamic models, within which the DD gradually increases up to an imposed maximum depth (80 km in the present work), has a significant effect on slab temperature evolution and hence allows for a more robust assessment of pre-steady state subduction thermal evolution.

Figure 2 demonstrates how thermal structure, convergence rates, trench migration, and slab dip co-evolve in the dynamic reference model of Holt and Condit (2021). The temporal evolution of these subduction properties is in broad agreement with various previous dynamic and/or time dependent modeling studies, as highlighted below. The earliest subduction phase (Figure 2a; up to \sim 8 Myr) is characterized by slow, few cm/yr convergence that gradually increases as the slab develops within the upper mantle and slab pull increases, that is, convergence velocity is largely controlled by the buoyancy contrast between the older, denser downgoing plate and the younger, warmer overriding plate and underlying asthenosphere. The intermediate phase of subduction (Figure 2b, \sim 8–17 Myr) is characterized by the highest convergence rates, paired with increasing slab dip and

EPSTEIN ET AL. 3 of 27

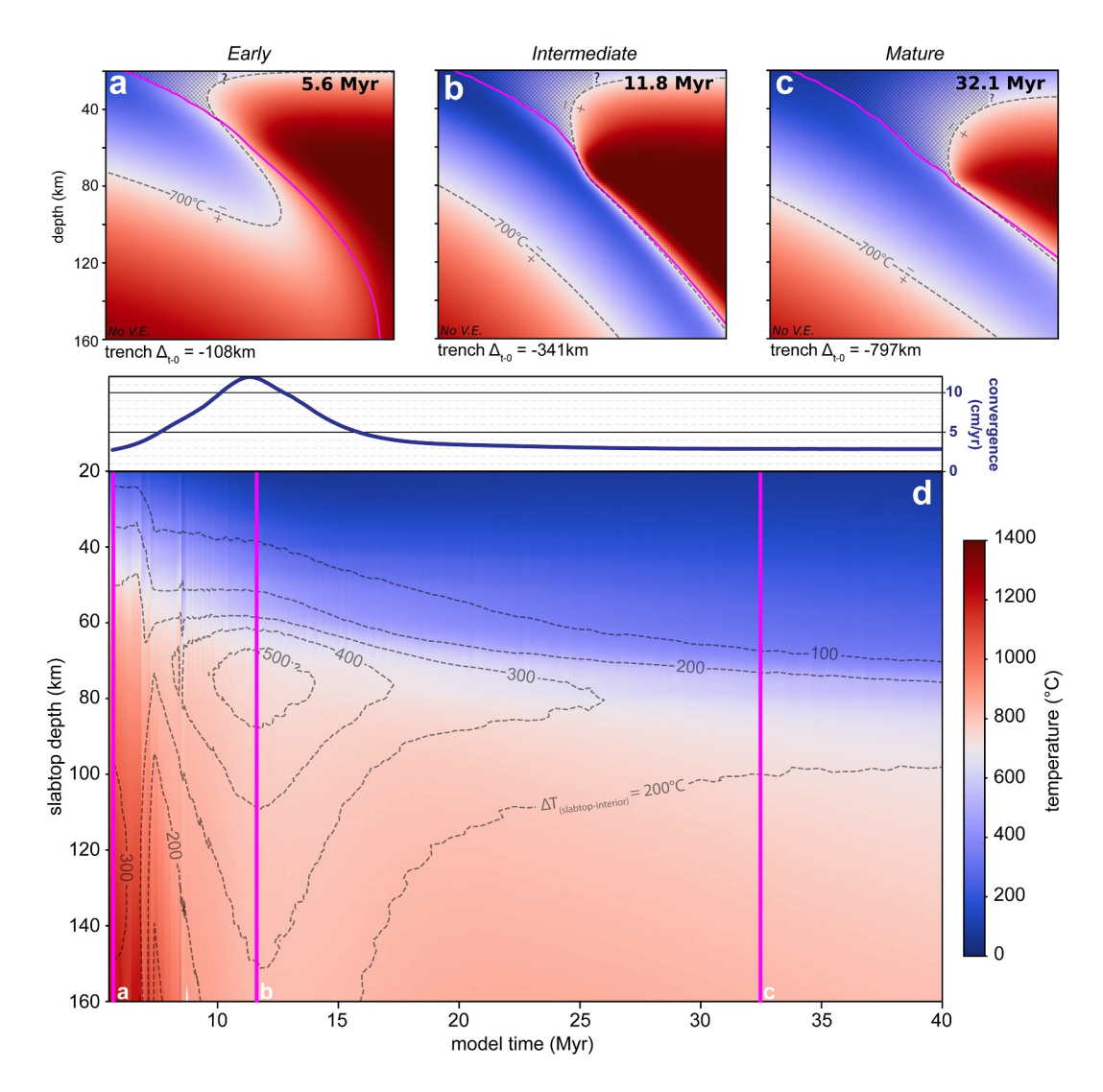


Figure 2. Thermal properties, trench migration, convergence rate, and slab top geometry of the reference model used in this study. (a–c) X-Y cross sections of temperature profiles corresponding to early, intermediate, and mature subduction, plotted with no vertical exaggeration. Magenta lines are the slab top, dashed gray line corresponds to the 700°C contour, and the cross hatches correspond to the region in the wedge where volumetrically significant hydrous minerals are potentially stable. The maximum depth of hydrous phase stability is not fixed but grows systematically with progressive forearc cooling from the descending slab. Trench Δ_{t-0} represents the trench offset from initial model conditions due to slab rollback. (d) Timeseries of convergence velocity at the trench (top), slab top temperature (colorbar), and slab thermal gradient (contours) as a function of slabtop depth. Magenta lines correspond to the three time slices shown in (a–c). Gradient contours correspond to temperature difference between the slab top and a point at 5 km depth within the slab. The slab top displays a general decrease in temperature at a given depth with increasing time. The thermal gradient within the slab is controlled largely by the convergence rate and demonstrates a very high gradient of >100°C/km at 12 Myr and 75 km depth.

trench migration, as the now-established slab sinks rapidly through the relatively weak upper mantle (e.g., Enns et al., 2005; Čížková & Bina, 2013). Lastly, quasi-steady state conditions in convergence and slab dip are achieved after the leading edge of the downgoing slab has bent backwards (i.e., flattened) atop the upper to lower mantle viscosity increase at 660 km depth (Figure 2c; Agrusta et al., 2017). Similar slab geometries are attained in many previous subduction models (e.g., Christensen, 1996; Holt et al., 2015) and observed at many Earth subduction zones (e.g., Goes et al., 2017; C. Li et al., 2008). Critically, this convergence rate evolution is observed regardless of whether the slab flattens at, or penetrates, the 660 km discontinuity (e.g., Garel et al., 2014). Hereafter, we term these three phases "early," "intermediate," and "mature" subduction.

The geometric and kinematic parameters detailed above dictate slab and mantle wedge temperatures (e.g., Kirby, 1995; Peacock & Wang, 1999; van Keken et al., 2002); hence their progression results in a highly time dependent slab and mantle wedge thermal structure. During the early phase convergence is slow and the leading

EPSTEIN ET AL. 4 of 27

edge of the slab is interacting with a (relatively) unperturbed mantle geotherm. The feedback between slow velocities and a warm mantle culminates in models predicting high temperatures in the slab and wedge (Figures 2a and 2d; Arcay et al., 2005; Zhou & Wada, 2021). The intermediate phase is associated with cold slab interiors (due largely to high convergence; Kincaid & Sacks, 1997), and progressive cooling of the slab top and mantle wedge (in the reference model due largely to the dynamic increase in DD; Figures 2b and d; Holt & Condit, 2021). The thermal contrast between the cold slab interior and the hot (but cooling) mantle wedge produces large thermal gradients within the slab (contours in Figure 2d). Mature subduction, marked by attainment of quasi-steady state kinematic and geometric conditions, is similarly associated with an approach to time-invariant thermal conditions in the slab and mantle wedge (Figures 2c and 2d; Zhou & Wada, 2021).

In summary, the Holt and Condit (2021) reference model exhibits a highly time-dependent thermal evolution that shares first-order features with other dynamic subduction models. In such models, subduction consists of an early and hot phase, an intermediate (and thermally transient) free sinking phase, and a mature phase where convergence rate and temperature are tied to interactions between the slab and the 660 km discontinuity (Figure 2; Figure S2 in Supporting Information S1). We use this dynamic thermal model to explore first-order controls on forearc mantle wedge hydration. We find that this hydration is intimately tied to the temperature-dependence of aqueous fluid release and of mantle wedge H_2O storage capacity, and that hydration extent is enhanced by the consideration of pre-steady state thermal variations.

2.2. The Hydrated Mantle Wedge

Direct observation or inference of mantle wedge hydration is accomplished via geophysical methods that rely on the known physical and thermodynamic properties of serpentine-group minerals. Serpentinization of a peridotite protolith leads to a decrease in density, variations in bulk elastic properties, and often to the production of magnetite: all of which impact geophysical observables (gravity anomalies, seismic velocities, and magnetic susceptibility, respectively; Blakely et al., 2005; Christensen, 1966; Carlson & Miller, 2003; Escartin et al., 2001; Evans, 2008; Frost & Beard, 2007). Geophysical evidence in support of a serpentinized mantle wedge initially came from the observation that the downdip limit of megathrust seismogenesis along cold margins coincided with the upper plate crust-mantle boundary (the Mohorovičić discontinuity, Moho for short), suggesting that the presence of weak hydrous phases in the mantle wedge leads to cessation of seismicity (Oleskevich et al., 1999; Peacock & Hyndman, 1999; see also Seno, 2005; K. Wang et al., 2020 for more recent discussion). Seismic tomography and receiver function studies subsequently demonstrated a decrease in P and S wave velocities in the mantle wedge and an inverted velocity perturbation across the upper plate Moho (Abe et al., 2013; Bostock et al., 2002; X. Li et al., 2003; Sodoudi et al., 2006, 2011). Seismological inferences of crystallographic preferred orientation have also been used to infer the presence of anisotropic hydrous minerals in the forearc mantle wedge (Bezacier et al., 2010; Katayama et al., 2009; Nagaya et al., 2016). Gravity and magnetic observations, often paired with seismic studies, infer serpentinization (Blakely et al., 2005; Doo et al., 2016; Tozer et al., 2017) and electromagnetic methods commonly identify a forearc conductive anomaly near the upper plate Moho associated with conductive free fluids (Worzewski et al., 2011) that are likely to be in equilibrium with wedge serpentinites (Reynard et al., 2011). When these complementary methods are combined for a single margin (e.g., Japan; C. F. Li, 2011), the case for serpentinization is often bolstered.

Additional evidence for the presence of serpentinized forearc mantle comes from exhumed materials from fossil subduction zones where many high-pressure rocks are enveloped within a serpentinite matrix (Guillot et al., 2001; Schwartz et al., 2001). In models of exhumation, dense eclogite blocks are exhumed due to entrainment in a lower-density serpentinite channel (Beaumont et al., 1999; Ernst, 2005). Evidence in support of this updip channel-transport comes from the observation that eclogite blocks exhumed during the middle phases of subduction rarely (if ever) record temperatures greater than serpentine breakdown (Agard et al., 2009; Hermann et al., 2000). In many cases matrix serpentinites also record geochemical signatures consistent with mantle wedge formation (e.g., Deschamps et al., 2013; Martin et al., 2020).

Geophysical evidence for wedge hydration is not noted at every subduction margin, or is still debated for some (Halpaap et al., 2019; cf. DeShon & Schwartz, 2004; MacKenzie et al., 2008), but appears to be present to some degree at most subduction zones (see Table S2 for a compilation of inferred serpentinization extents). Models of wedge hydration extents inferred from kinematically driven models rely on steady state fluid release from the slab, which largely occurs at or below the DD (Abers et al., 2017; Hacker et al., 2003; van Keken et al., 2011). Yet,

EPSTEIN ET AL. 5 of 27

in dynamic models, the period of subduction leading up to steady state is characterized by very large temperature variations within the slab and mantle wedge that may favor hydration. Here, we explore the influence of a time-evolving subduction zone thermal structure on the hydration of the forearc mantle wedge to test the hypothesis that the bulk of mantle wedge hydration may occur in the early to intermediate stages of subduction, prior to attainment of steady-state conditions. Even if the magnitudes of thermal variability are unique for each subduction zone, the general stages of evolution should be taken as the rule, not the exception (e.g., Faccenna et al., 2001; Stern & Bloomer, 1992; Zhou & Wada, 2021). Thus, while we present results from four similar but distinct model setups, we argue that the subduction zone thermal evolution, and the resulting wedge hydration systematics, are widely applicable to the global range of subduction zones.

3. Methods

We couple phase equilibria modeling with the time-evolving thermal structure (as predicted by the geodynamic models) both within the slab to quantify predicted slab dehydration, and within the overlying mantle wedge to quantify predicted mantle hydration. For each individual timestep the method to determine slab dehydration and wedge hydration is similar to previous studies (e.g., Abers et al., 2017; Epstein et al., 2021; van Keken et al., 2011; Wada et al., 2012) and uses the modeled thermal field to determine how much $\rm H_2O$ is liberated from the slab and over what cross-sectional area of the mantle wedge hydrous mineral phases can be stable. This approach is integrated over all of the model timesteps to observe how the $\rm H_2O$ source (slab) versus sink (wedge) relations evolve through time. We further generalize our model by exploring the effect on wedge hydration of adding a subducted sedimentary section and/or changing the strength of the subducting crust.

3.1. Geodynamic Model

We use the geodynamic models of Holt and Condit (2021); these are dynamic and time-dependent subduction models constructed using the finite element code ASPECT (v2.1.0; Bangerth et al., 2020a, 2020b; Heister et al., 2017; Kronbichler et al., 2012). The model solves the equations for conservation of mass, momentum, and energy for an incompressible viscous fluid (Boussinesq approximation) within a 2-D domain with dimensions of 11,600 × 2,900 km and boundaries that are mechanically free-slip (Figure S1 in Supporting Information S1). These models simulate intra-oceanic subduction with an initially 90 Ma subducting plate descending beneath a 10 Ma overriding plate (i.e., the plates are oceanic and differ only in age). Both plates are initially defined by halfspace cooling profiles that describe the thermal structure of the cold plates relative to the surface $(0^{\circ}C)$ and mantle (potential temperature of 1,421.5°C; Stein & Stein, 1992). The downgoing plate has an initial length of 6,000 km, and is capped by an 8 km thick, isoviscous crustal section. The model considers a composite mantle rheology defined by diffusion creep of olivine (whole domain), dislocation creep of olivine (upper mantle), and plastic yielding (within the lithospheric plates). Diffusion and dislocation creep constants are set to fall within the range of experimental values for dry olivine (Hirth & Kohlstedt, 2003; Karato & Wu, 1993). The viscosity increases ~30 fold at the upper-to-lower mantle transition; within the range determined based on geoid constraints (e.g., Hager, 1984). For a full description of the dynamic thermal model setup and all parameter values, the reader is referred to Holt and Condit (2021).

Subduction initiates soon after the model run begins and is facilitated by the relative negative buoyancy of the subducting plate and an imposed weak layer that crosscuts the lithosphere, as is broadly consistent with initiation occurring along a transform fault or during passive margin collapse (Stern, 2004). The DD gradually increases through time until it reaches a depth of 80 km. At this depth the imposed weak layer is eliminated, effectively imposing a maximum DD. The evolution of convergence rate, slabtop temperature, and slab temperature gradients are displayed in Figure 2 (see also Figures S1 and S2 in Supporting Information S1).

In the current study, we analyze two subduction models: one with a "weak" crust $(2 \times 10^{20} \, \text{Pa} \, \text{s})$; Holt and Condit's reference model), and one with a "strong" crust $(4 \times 10^{20} \, \text{Pa} \, \text{s})$. As explored by Behr et al. (2022), with similar model setups, an increased crustal viscosity reduces subduction zone convergence rates by increasing the subduction-resisting interface shear force (cf. Behr & Becker, 2018) and therefore pushes the various subduction phases to significantly later times (e.g., peak convergence after ~20 Myrs of the model evolution, relative to ~11 Myrs in the weaker crust reference, cf., Figure 2 and Figure S2 in Supporting Information S1). We therefore examine the effects of variable oceanic crustal strengths to explore whether or not our predicted trends in mantle wedge hydration are independent of differences in convergence rates (themselves dependent on crustal strength)

EPSTEIN ET AL. 6 of 27

2576604x, 2024, 4, Downloaded

com/doi/10.1029/2023AV001121 by University Of Miami Libraries,

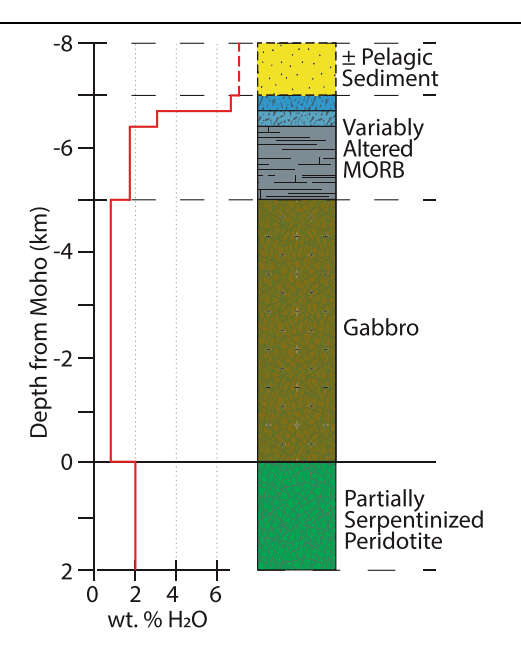


Figure 3. Subducted lithologies, thicknesses, and initial water contents for model inputs and phase equilibria calculations as a function of depth from the downgoing plate moho.

that, in turn, strongly impact slab temperature (e.g., Peacock, 1996). In our modeling, increasing the crustal strength by a factor of 2 reduces convergence rates by an average of 44%, 64%, and 17% during early, intermediate, and mature phases, respectively (cf., Figure 2 & Figure S2 in Supporting Information S1).

Slab and forearc thermal conditions were extracted from the models between 5.6 and 40 Myr after subduction initiation for the weak crust case, and between 7.0 and 40 Myr for the strong crust case, extending from the surface to 225 km depths. Between these times, we analyze every 50th numerical timestep; this corresponds to average time intervals of 0.5 and 0.7 Myrs for the weak and strong crust models, respectively. The first 5.6 and 7.0 Myr of modeled subduction are ignored to reduce the imprint of the initial thermal conditions and specific subduction initiation mechanism on our analysis. Thus, we begin our analysis during young subduction rather than during initiation.

3.2. Phase Equilibria Modeling

The compositional layering of the downgoing slab is the same as used by Hacker (2008) and van Keken et al. (2011), consisting of 300 m of upper volcanic extrusives, 300 m of lower volcanic extrusives, 1,400 m of sheeted dykes, 5,000 m of gabbro, and 2,000 m of partially serpentinized peridotite (Figure 3). Composition of the extrusives and sheeted dykes are from Gale et al. (2013) with $\rm H_2O$ and $\rm K_2O$ contents determined from Jarrard (2003) for a 90 Myr slab. The gabbro composition is that of Dick et al. (2000) with 0.8 wt.%

 $\rm H_2O$, and partially serpentinized abyssal peridotite is from Niu (2004) with 2 wt.% $\rm H_2O$. For saturated peridotite of the forearc mantle wedge we use the composition for mantle wedge lherzolite determined in Deschamps et al. (2013). For the sediment-bearing models we include an additional 1 km of pelagic clay with compositions after van Keken et al. (2011; see also Plank & Langmuir, 1998). Recent geophysical investigations have demonstrated large variability in extents of incoming plate hydration state, particularly in the serpentinized peridotite layer (Arnulf et al., 2022; Cordell et al., 2023). As demonstrated in the results section, peridotites of the downgoing plate do not significantly contribute to wedge hydration, and we present results pertaining to a single (relatively conservative) hydration state to best allow for comparison to previous models (invoking the same hydration states), and to demonstrate that the proposed wedge hydration mechanism does not require extensive hydration of the incoming plate.

Mineral-bound water content as a function of *P-T* conditions were modeled using the Gibbs free energy minimization software Perple_X for each of the above listed compositions (version 7.0.1; Connolly, 2005). Calculations were made in the system Na₂O-CaO-K₂O-FeO-MgO-Al₂O₃-SiO₂-H₂O, with H₂O as the only mobile component. The thermodynamic database used is that of Holland and Powell (2011), and we used the fluid equation of state of Pitzer and Sterner (1994). Solid solution models and pseudosections for all calculations can be found in the supplementary file (Table S1, Figures S4–S7 in Supporting Information S1; see also Data Repository: Epstein, 2024).

3.3. Slab Dehydration

We calculated the total mass of H_2O liberated from the slab predicted by the thermodynamic models for each time step in the geodynamic models, assuming vertical and channelized fluid transport (see Data Repository for code). The results for each time step are then integrated over the lifetime of the subduction models. The slab has a total initial thickness of 9 km of partially hydrated material not including the sediment section. This is discretized into 100 m elements (extending from the slabtop to 9 km depth) with a 1 km spacing in the horizontal (X) direction. The X and vertical (X) coordinates and the temperature, pressure, density, and X0 content for each element (based on the lithology present) are extracted from the model for each time step analyzed. For a given time step, the mass of X0 released from the slab per unit volume of material (X0 the same depth from the difference in mineral-bound X1 the same depth from the slabtop. Taking the slab dip and convergence rate into account, we calculate the X2 released from each element

EPSTEIN ET AL. 7 of 27

per year and sum this value over the vertical thickness of the slab (slab thickness of 9 km times cosine of dip) to determine the H_2O production in kg/yr per meter trench length for each time step as a function of distance from the trench. This approach is performed for every time step and is then integrated using the time difference between each time step to obtain an estimate of H_2O produced through time as a function of distance, and by extension, as a function of depth. The approach for monitoring dehydration for a given time step is similar to the "uniform hydration" method presented by Wada et al. (2012; i.e. no rehydration within the downgoing plate), and to the method employed by Epstein et al. (2021) but differs by incorporating temporal variation.

3.4. Wedge Hydration

Using the thermal field of the forearc and the pseudosection of the saturated lherzolite, we also determine the cross-sectional areas over which serpentine and other hydrous phases are stable within the wedge for each time step and determine the mass of water that can be stored within these minerals over the P-T conditions of the model. This latter value defines the absolute mass of H_2O that could be bound within minerals in the forearc mantle wedge, which we term the H_2O capacity (analogous to the method outlined in Abers et al., 2017). The H_2O capacity does not reflect the extent of mantle wedge hydration. Modeled hydration extents are also dependent on slab dehydration occurring directly beneath the region of the wedge where hydrous minerals are stable, as discussed below (i.e., aqueous fluid availability). Where quantitative predictions are made, we use the term hydration ratio in place of hydration extent.

We have assumed a horizontal upper plate moho at a depth of 30 km which imposes a shallow end limit on fluid contribution to mantle wedge hydration (i.e., no H_2O addition to the wedge if dehydration occurs at depths less than 30 km). Early in the model, the downdip limit of wedge hydration is determined by where the slabtop P-T path intersects the anhydrous peridotite phase boundary in our calculated pseudosection, such that this limit increases in depth with progressive forearc cooling (see results). However, once the downdip limit of hydrous phase stability is equal or greater than 80 km we pin the limit to this depth. This depth coincides with the maximum decoupling depth (MDD) inferred from surface heat flow measurements which, in turn, suggests that mature subduction zone slabs become fully coupled to the overlying mantle and hence undergo rapid heating at around 80 km depth (Furukawa, 1993; Gao & Wang, 2014; Syracuse et al., 2010; Wada & Wang, 2009).

We do not consider wedge hydration immediately beneath the upper plate Moho in the arc and backarc region, as this would involve consideration of partial melting and two-phase fluid transport (question marks at shallow depths in Figures 2a–2c). Thus, we define a relatively strict region for the hydratable mantle wedge in the present model: the region lying vertically above the descending slab from depths of 30 km to the downdip limit of chlorite stability along the plate interface or 80 km, whichever is less. Where fluid is produced in the slab at depths directly beneath serpentine or chlorite stability in the wedge, we assume perfectly efficient fluid transfer into the wedge and complete uptake into the hydrous mineral phase or phases stable in the wedge, as implemented in previous studies (Abers et al., 2017; van Keken et al., 2011; Wada et al., 2012). The hydratable wedge is therefore treated as a single, connected reservoir: 100% of fluid that enters the hydratable region contributes to hydration. This model does not factor in volume change associated with serpentinization, nor do we account for mass advection out of the mantle wedge associated with trench migration or any other processes.

4. Results

We analyze the results of the two separate subduction models, one with a weaker subducting crust $(2 \times 10^{20} \text{ Pa s})$; the Holt and Condit reference model), and one with a stronger crust $(4 \times 10^{20} \text{ Pa s})$. For each crustal strength, we performed dehydration calculations of the downgoing lithosphere with two different lithologic constructions of the slab crust shown in Figure 3: (a) a purely igneous crustal section without metasedimentary cover, and (b) igneous crust with 1 km of pelagic, initially clay-rich, (meta)sediment. We thus present model results of slab dehydration and forearc hydration for four distinct combinations of crustal strength and lithologic architecture computations (lithologic framework shown in Figure 3). Where shorthand is appropriate, we use "W" and "S" to signify weak versus strong crust and "n" and "s" to signify non-sediment versus sediment bearing models such that the four models can be written as Wn, Ws, Sn, and Ss (weak non-sediment, weak with sediment, strong non-sediment, and strong with sediment, respectively).

EPSTEIN ET AL. 8 of 27

2576604x, 2024, 4, Downloaded from https://agupubs.onlinelibrary.wiley.com/doi/10.1029/2023AV001121 by University Of Mami Libraries, Wiley Online Library on [26/07/2024]. See the Terms and Conditions (https://onlinelibrary

and-conditions) on Wiley Online Library for rules of use; OA articl

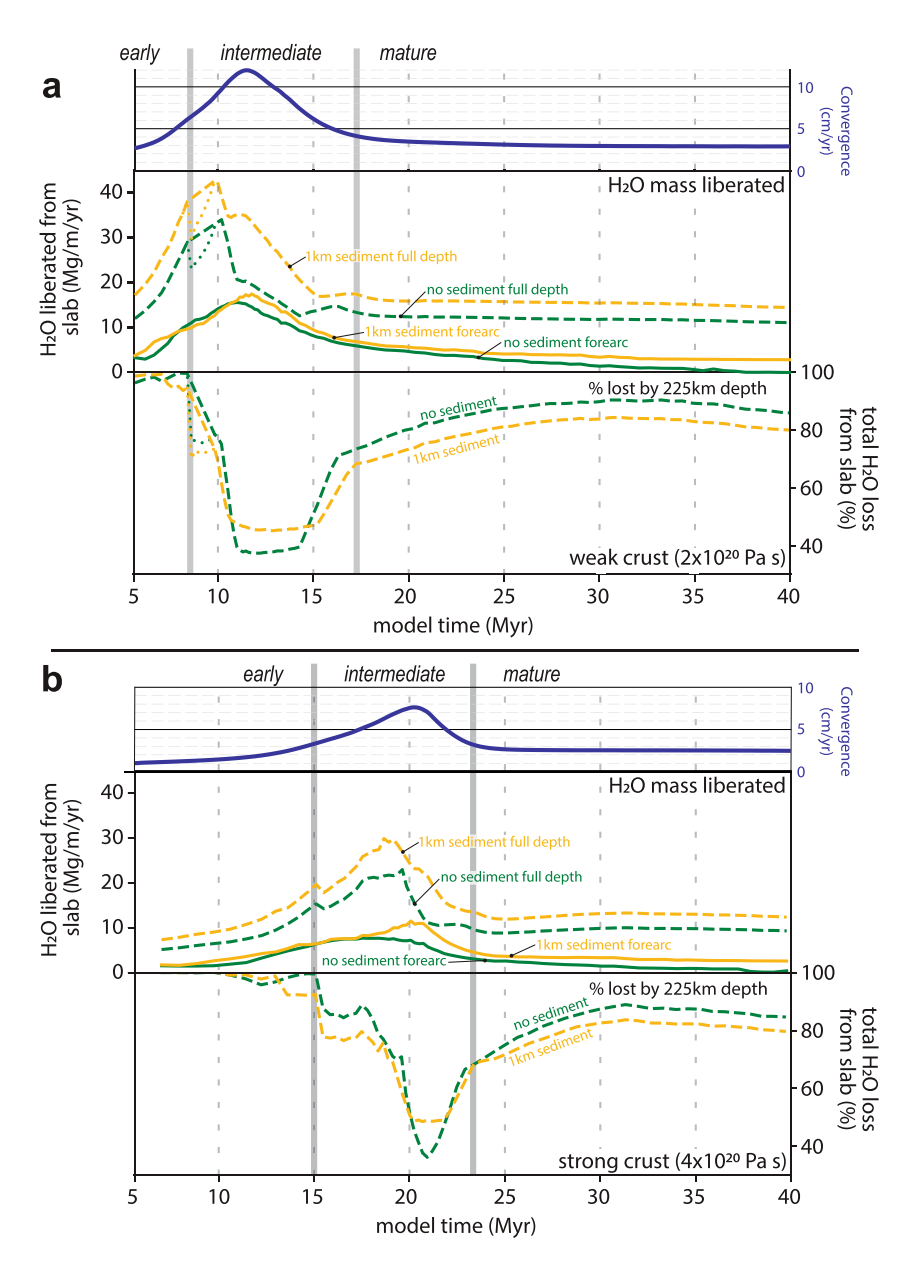


Figure 4. Mass and mass fraction of fluid released from the slab. (a) Mass of fluid released per year over the entire model range (dashed lines) and within the forearc (solid lines) for the weak crustal cases with and without a sedimentary section (yellow and green, respectively). The lower panel shows the fraction of fluid liberated from the subducted slab over the entire model range and is used to define subduction phases. (b) Mass of fluid released for the strong crustal cases. Both figures show dependence on convergence rate (blue lines above a, b). Dotted lines are model artifacts from the interpolation algorithm, with the overlying dashes being interpolations. Interpolations do not affect forearc fluid release. Upper panel units are Mg/yr per meter trench length (1 Mg = 10^6 g).

4.1. Full Depth Slab Dehydration (0-225 km Depths)

Figure 4 shows the evolving convergence rate (top panels) as well as the amount of mineral-bound H_2O that is predicted to be released from the slab over the entire model as a function of time for both weak and strong crustal cases (Figures 4a and 4b, respectively). The center panels record H_2O -fluid release as absolute amounts (dashed lines for full model depth, solid lines for forearc release), and the bottom panels as a percentage of mineral bound H_2O within the downgoing slab. The systematics shown in Figure 4 provide a phenomenological basis for the separation of subduction time periods adopted here (see labels above top panels). Early subduction is defined as

EPSTEIN ET AL. 9 of 27



Table 1

Model ^a	Wn	Ws	Sn	Ss	Figure
Intermediate phase age range (Myr)	8.0–17.5		15.0–24.0		Figure 4
Maximum convergence at trench (cm/yr) (age of max convergence, Myr)	12.0 (11.3)	12.0 (11.3)	7.6 (20.3)	7.6 (20.3)	Figures 2 and 4
Max. slab H_2O production: full depth (Mg/yr/m) (age, Myr)	33.0 (10.2)	43.0 (9.8)	22.2 (19.8)	30.0 (18.8)	Figure 4
Max. slab H_2O production: forearc (Mg/yr/m) (age, Myr)	15.4 (11.0)	17.4 (11.8)	7.7 (18.0)	11.5 (20.0)	Figures 4 and 9
Maximum hydration ratio (%) (age, Myr)	64 (14.3)	71 (<i>14.3</i>)	30 (22.5)	38 (22.5)	Figure 10
Slab H ₂ O prod. at 40 Myr: forearc (Mg/m/yr)	0.0	2.9	0.1	2.6	Figures 4 and 9
Mantle wedge H ₂ O capacity at 40 Myr (Tg/m)	518		463		Figure 7, Figure S6 in Supporting Information S1
Hydration ratio at 40 Myr (%)	32	43	22	33	Figure 10

^aItalic values in parentheses refer to timing of maxima in Myr.

the period where the downgoing slab is sufficiently heated such that there is complete removal of mineral-bound $\rm H_2O$ within the upper mantle (<225 km). The intermediate period is defined as the range over which convergence rates are highest and there is thus maximum retention of mineral-bound $\rm H_2O$ within the slab to depths beyond the model range (>225 km). Mature subduction is defined as the period beyond this where convergence rate is strongly controlled by interaction between the slab and the 660 km discontinuity and dehydration varies slowly or is relatively constant. See Table 1 for a summary of model results.

Temporal variability of slab dehydration within the models is best visualized as a time series of H₂O fluid production as a function of slabtop depth (Figure 5). For a given model time (X-axis), the shading corresponds to the magnitude of H₂O fluid released from the subducting slab at a given slabtop depth (i.e., all dehydration within a vertical column projected onto the slabtop). During the early subduction phase initial slabtop temperatures are high, and the slab is hot throughout (e.g., for the weak crust case slabtop $T \approx 700^{\circ}$ C at 40 km depth, $\Delta T_{\rm slabtop-interior} \approx 250$ °C, Figure 2d; see Figure S2 in Supporting Information S1 for the strong crust case). For the non-sediment, weak crust model (Wn) dehydration begins at a slabtop depth of ~ 25 km during the early phase of subduction (Figure 5a). As the model approaches quasi steady state conditions, the onset of dehydration gradually progresses to slabtop depths of >80 km. The shallowest fluid released from the slab for all model times (<100 km depth, i.e., within the forearc) is dominantly derived from dehydrating metabasalts and is greatest during the intermediate phase (~8–17.5 Myr; Figure 5a), which is consistent with the results of Holt and Condit (2021). Partially serpentinized peridotite and gabbro of the slab undergo dehydration beyond forearc depths, mostly at depths greater than 130 km (annotations in Figure 5a), and at no time contribute to forearc wedge hydration. Slab dehydration occurring within the forearc during the early subduction phase is due to the breakdown of greenschist facies mineral assemblages (e.g., pumpellyite, stilpnomelane, and chlorite breakdown) with lesser involvement of amphibole breakdown at the highest temperatures. During the intermediate and mature stages, the slab undergoes dehydration due to destabilization of sodic amphibole and lawsonite at blueschist facies metamorphic P-T conditions, together with lesser contributions from dehydration associated with breakdown of chlorite and talc (Figure S4 in Supporting Information S1).

In the weak crust, sediment-bearing case (Ws) dehydration systematics are generally consistent with the non-sediment cases with the addition of some continued shallower dehydration sourced from metasediments (Figure 5b). Early subduction phase sediment dehydration is due to breakdown of stilpnomelane, white mica, and biotite, whereas dehydration during intermediate to mature stages of subduction is due to breakdown of stilpnomelane, lawsonite, and amphibole (Figure S5 in Supporting Information S1). Due to refrigeration of the slab by the sedimentary cover, dehydration of the altered basalt occurs at slightly greater depths (+5-10 km) than in non-sediment cases and is slightly more diffuse but is caused by the same mineral reactions as discussed in the previous paragraph. The dominant pulse of forearc H_2O fluid release again occurs during the

EPSTEIN ET AL. 10 of 27

2576604x, 2024, 4, Downloaded from https://agupubs.onlinelibrary.wiley.com/doi/10.1029/2023AV001121 by University Of Mami Libraries, Wiley Online Library on [2607/2024]. See the Terms and Conditions (https://doi.org/10.1029/2023AV001121 by University Of Mami Libraries, Wiley Online Library on [2607/2024]. See the Terms and Conditions (https://doi.org/10.1029/2023AV001121 by University Of Mami Libraries, Wiley Online Library on [2607/2024]. See the Terms and Conditions (https://doi.org/10.1029/2023AV001121 by University Of Mami Libraries, Wiley Online Library on [2607/2024]. See the Terms and Conditions (https://doi.org/10.1029/2023AV001121 by University Of Mami Libraries, Wiley Online Library on [2607/2024]. See the Terms and Conditions (https://doi.org/10.1029/2023AV001121 by University Of Mami Libraries, Wiley Online Library on [2607/2024]. See the Terms and Conditions (https://doi.org/10.1029/2023AV001121 by University Of Mami Libraries, Wiley Online Library on [2607/2024]. See the Terms and Conditions (https://doi.org/10.1029/2023AV001121 by University Of Mami Libraries, Wiley Online Library on [2607/2024]. See the Terms and Conditions (https://doi.org/10.1029/2023AV001121 by University Of Mami Libraries, Wiley Online Library on [2607/2024]. See the Terms and Conditions (https://doi.org/10.1029/2023AV001121 by University Of Mami Libraries, Wiley Online Library on [2607/2024]. See the Terms and Conditions (https://doi.org/10.1029/2023AV001121 by University Of Mami Libraries, Wiley Online Library on [2607/2024]. See the Terms and Conditions (https://doi.org/10.1029/2023AV001121 by University Of Mami Libraries, Wiley Online Library on [2607/2024]. See the Terms and Conditions (https://doi.org/10.1029/2023AV001121 by University Of Mami Libraries, Wiley Online Library on [2607/2024]. See the Terms and Conditions (https://doi.org/10.1029). See the

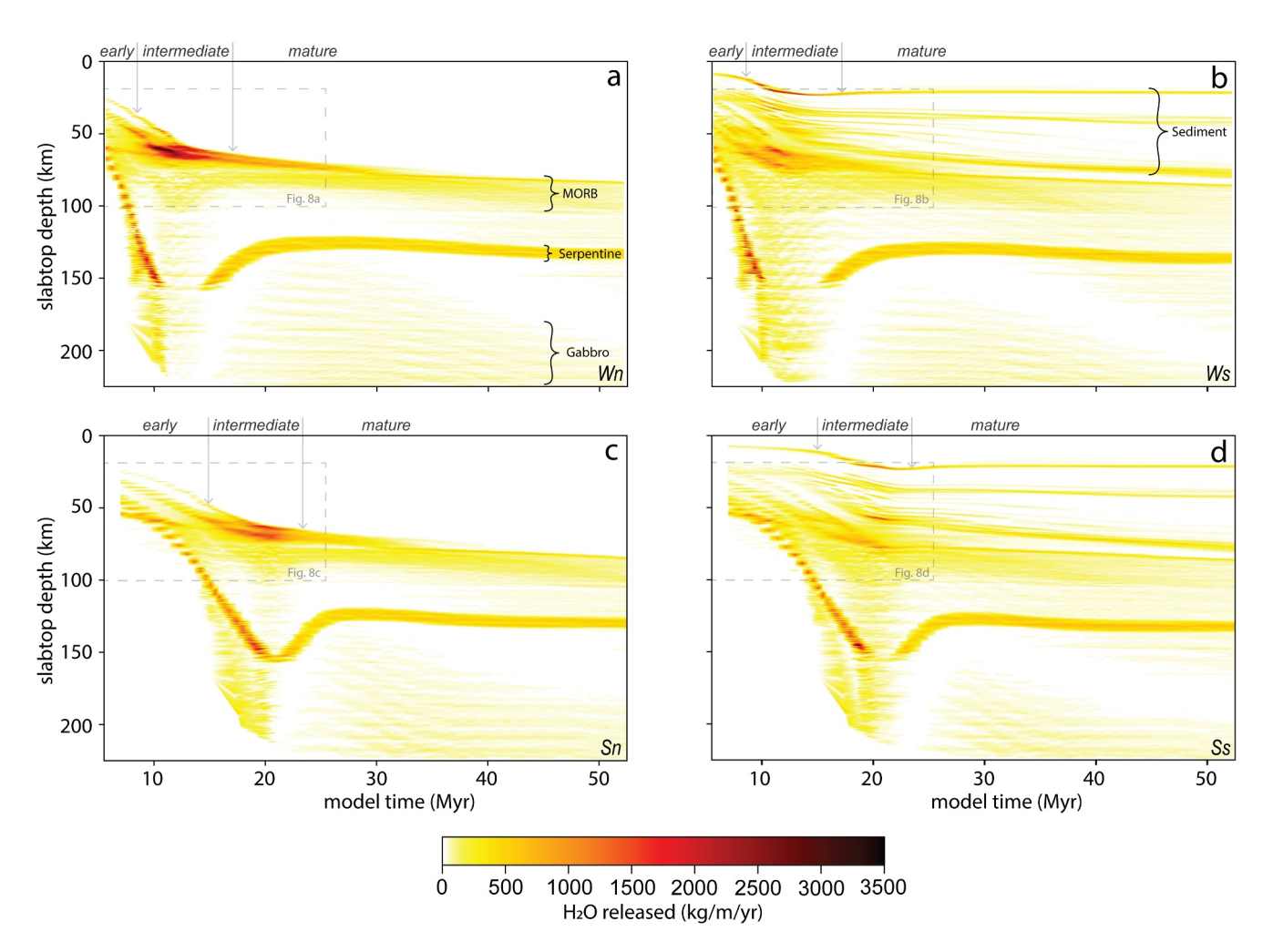


Figure 5. Time series of depth of dehydration and mass of H_2O released in kg/yr per meter trench length. (a) Forearc dehydration in the weak crust non-sediment case (Wn) occurs due to hydrous-mineral breakdown in altered basalts and is greatest during the intermediate phase at slabtop depths of 50–70 km. (b) The weak crust sediment-bearing case (Ws) contains an added 1 km of pelagic sediment and demonstrates more extensive forearc dehydration throughout the model run. (c) The strong crust non-sediment case (Sn) demonstrates peak forearc dehydration during the intermediate phase which occurs \sim 7 Myr later than for the weak crust case. (d) The strong crust sediment-bearing (Ss). For all models, serpentine and gabbro dehydration occur at subarc or backarc depths, as labeled in panel (a).

intermediate phase. With the addition of sediment, there is little to no noticeable change in serpentinite and gabbro dehydration.

For the strong crust cases (Sn and Ss) the timing of maximum slab dehydration occurs 8–10 Myr later than in the weak crust cases (Figures 5c and 5d, Table 1). Aside from this temporal shift, the strong crust cases have the same overall dehydration systematics as the equivalent weak crust cases, albeit with lower magnitudes of H_2O fluid release (cf. Figures 5a and c; Figure S3 in Supporting Information S1). Maximum values of forearc dehydration flux range from \sim 1,000 kg/yr per m trench length (Ss) to \sim 3,500 kg/yr per m trench length (Ss), occurring at slabtop depths of \sim 60 km at 11 and 20 Myr, respectively (Figure 4).

4.2. Wedge Hydration

4.2.1. Hydration Topology of Peridotites and Wedge H₂O Capacity

The extent of wedge hydration (ratio between mantle wedge bound $\rm H_2O$ and $\rm H_2O$ capacity) is, in principle, dependent on the availability of free $\rm H_2O$ (previous section) and on the predicted stability of hydrous mineral phases within the mantle wedge. Phase equilibria modeling reveals the potential extent of hydration in P-T space of the mantle wedge (Figure 6). Addition of water to the point of saturation of the mantle wedge produces the assemblage serpentine (antigorite/lizardite) + brucite at temperatures <450°C and contains 12–14 wt.% $\rm H_2O$ over

EPSTEIN ET AL. 11 of 27

2576604x, 2024, 4, Downloaded from https://agupubs.onlinelibrary.wiley.com/doi/10.1029/2023AV001121 by University Of Miami Libraries, Wiley Online Library on [2607/2024]. See the

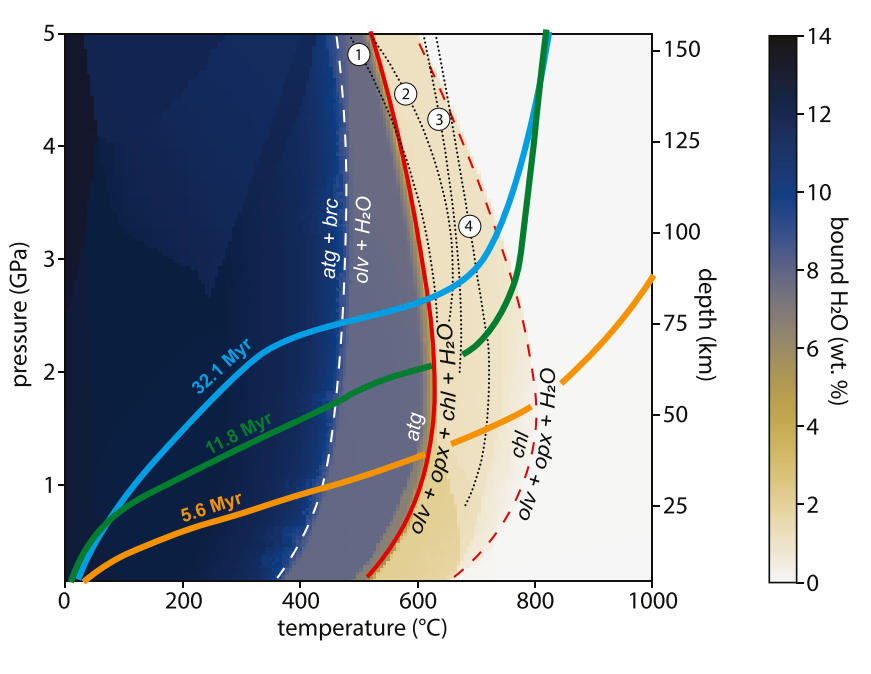


Figure 6. Pseudosection color-shaded for mineral-bound water content in saturated peridotite of the forearc mantle wedge. The main dehydration reactions with increasing temperature are indicated with dashed white, solid red, and dashed red lines and correspond to brucite-out, antigorite-out, and chlorite-out, respectively. The *P-T* paths for the three time slices shown in Figure 1 are shown as thick, labeled, colored lines. Thin dotted, numbered, lines correspond to experimental estimates of the upper limit of antigorite in ultramafic rocks: (1) low-Al antigorite of Bromiley and Pawley (2003), (2) Wunder and Schreyer (1997), (3) high-Al antigorite of Bromiley and Pawley (2003), (4) Ulmer and Trommsdorff (1995).

the depth range of interest. Extending from 450°C to $600\text{-}625^{\circ}\text{C}$ antigorite + olivine is stable with ~ 8 wt.% H_2O , after which chlorite + olivine + orthopyroxene is stabilized at the expense of antigorite. Between 700 and 800°C , chlorite is destabilized, producing the nominally anhydrous final assemblage olivine + orthopyroxene (Figure 6). The destabilization of chlorite marks the upper limit of volumetrically significant hydrous phase stability in the mantle wedge, with only minor amounts of biotite and/or talc stable beyond this temperature, and only at pressures ≤ 2 GPa. These minerals are not considered further as major carriers of H_2O in the wedge.

Combining these results above with the evolving forearc thermal structure (Figure 2a–2c, Figure S2 in Supporting Information S1), we use our models to demonstrate the variation of H_2O capacity of the mantle wedge through time, defined as the maximum H_2O content that can be stabilized in hydrous minerals within the mantle wedge. For all tested models, the wedge H_2O capacity increases as the model progresses and the forearc undergoes cooling (Figure 7, Figure S6 in Supporting Information S1) culminating in quasi-steady state H_2O capacities comparable to values determined by Abers et al. (2017; median of 640×10^{12} g/m H_2O over 56 margins compared to 463 and 518×10^{12} g/m for the strong and weak crust cases, respectively; Table 1, Figure 7, and Figure S6 in Supporting Information S1). The ratio of forearc slab H_2O production to mantle H_2O capacity through time (next section) represents the modeled hydration ratio of the mantle wedge.

4.2.2. Slab to Wedge H₂O Exchange

We next compare the slab dehydration systematics of Figure 5 with the stability of hydrous minerals in the overlying mantle wedge (Figures 6 and 7) to determine when and where slab fluids will promote wedge hydration. Figure 8 compares the time-dependent systematics of slab dehydration with the stability of hydrous minerals within the mantle wedge (dashed lines) at a depth immediately above the plate interface (See subset boxes in Figure 5 for ranges displayed in Figure 8). For the non-sediment case, Wn, the main pulse of dehydration occurs entirely within the stability field of chlorite and largely also within the antigorite stability field, indicating that this timeframe is associated with the most rapid addition of H_2O to the mantle wedge at P-T conditions of hydrous mineral stability, together resulting in the most rapid hydration of the mantle wedge peridotite (Figure 8a). For the sedimentary cover case, Ws, the pulse is more diffuse due to shallow sediment dehydration as well as refrigeration of the underlying basalts. Due to this refrigeration, the large pulse occurs mostly within the chlorite stability field

EPSTEIN ET AL. 12 of 27

/agupubs.onlinelibrary.wiley.com/doi/10.1029/2023AV001121 by University Of Miami Libraries, Wiley Online Library on [26/07/2024]. See the

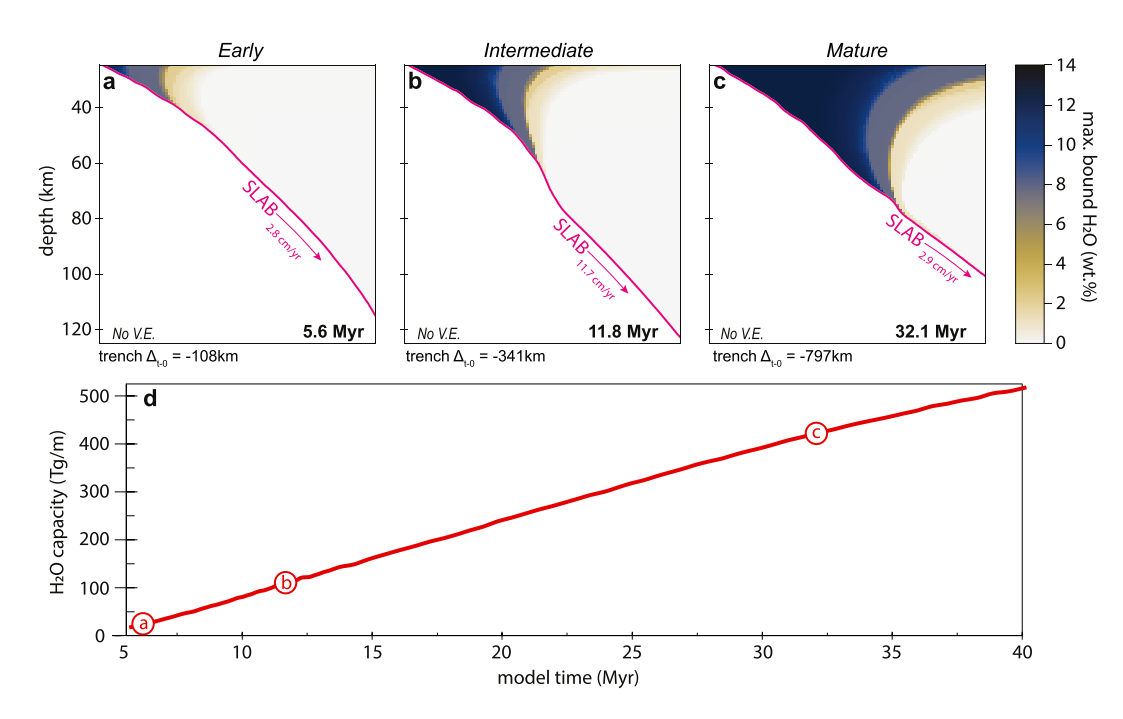


Figure 7. H_2O capacity of the forearc mantle wedge for the weak crust case. (a–c) X-Y cross sections at three timesteps through the mantle wedge corresponding to early, intermediate, and mature subduction, shaded according to bulk H_2O content (see Figure 6 for mineralogy). See Figure 2 caption for trench Δ_{t-0} definition. Cross sections have no vertical exaggeration. (d) Timeseries growth of wedge H_2O capacity, with letters signifying the corresponding cross section. Units are Tg/m of trench length (1 $Tg = 10^{12}$ g).

(Figure 8b). The strong crust cases, Sn and Ss, demonstrate very similar trends with respect to the stable mineral assemblages within the mantle wedge (Figures 8c and 8d).

Figure 8 additionally demonstrates that slab serpentinites do not undergo dehydration within the forearc (see annotation in Figure 8c). We further note that the antigorite solid solution model used in our calculations predicts deserpentinization at $\sim 100^{\circ}$ C less than experimental studies (dotted lines in Figure 6; Ulmer & Trommsdorff, 1995); this suggests that the *P-T* conditions adopted for wedge deserpentinization should be taken as a minimum, and that the region of antigorite + olivine stability may extend to higher temperatures than presently considered.

The magnitude of slab dehydration and a discrimination of the associated hydrous mineral assemblages that stabilize within the mantle wedge is displayed in Figure 9. The non-sediment cases demonstrate a general decrease through time of the percentage of slab-bound H_2O liberated in the forearc, with pronounced peaks of slab H_2O loss (as a percentage of mineral-bound H_2O) at the boundaries between subduction phases (shaded fields, left axis, Figures 9a and 9c). Slab dehydration results in wedge hydration within the chlorite and antigorite (plus olivine) fields in sub-equal proportions (e.g., at the intermediate-mature phase boundary of Figure 9a: 15% of the initially slab-bound H_2O contributes to stabilizing antigorite + olivine and 15% contributes to stabilizing chlorite). Notably, in the non-sediment case there is very little H_2O release at temperatures where brucite is stable. As the models progress, percentages of slab H_2O loss decrease to zero as steady-state conditions are approached.

The sediment-bearing cases have higher net H_2O release on a mass basis (red lines), but due to increased mineral-bound water content of the slab, record lower fractions of H_2O loss early in the models. In general, the Ws and Ss cases demonstrate slab fluids resulting in wedge hydration within the chlorite and antigorite stability fields during the early phase, with the antigorite + brucite field becoming dominant at intermediate and mature phases (Figures 9b and 9d). In both cases, the combined antigorite and antigorite + brucite fields accommodate the majority of the released H_2O corresponding to $\sim 15\%$ of the H_2O initially bound in the slab.

EPSTEIN ET AL. 13 of 27

2576604x, 2024, 4, Downloaded from https://agupubs.onlinelibrary.wiley.com/doi/10.1029/2023AV001121 by University Of Miami Libraries, Wiley Online Library on [26/07/2024]. See the Terms

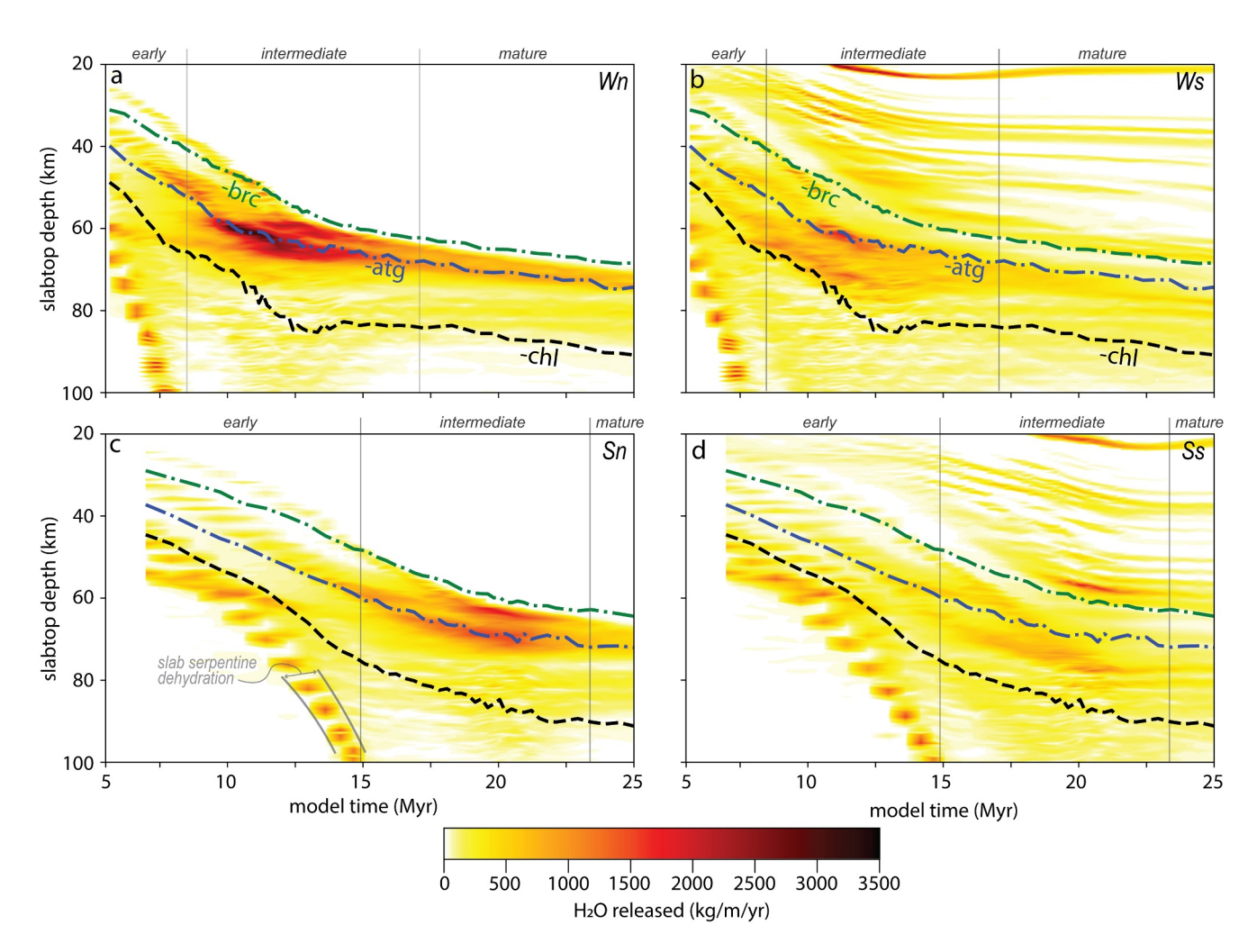


Figure 8. Forearc dehydration systematics and stability limits for hydrous phases in the mantle wedge adjacent to the subduction interface for the smaller region outlined in Figure 5. (a, b) Weak crustal cases. (c, d) Strong crustal cases. In all instances the major fluid pulse occurs within the forearc, whereas slab serpentine dehydration occurs above hydrous phase stability in the wedge, as expected given that slab interiors are cooler than slab tops. The sediment-bearing cases (b, d) demonstrate significant dehydration within the brucite stability field.

Maximum rates of H₂O delivery to the wedge from the slab peak during the intermediate phase of subduction. For both strength cases, as the models approach steady state, sediments are the sole forearc H₂O source. The non-sediment cases do not record any forearc dehydration at or beyond 40 Myr, similar to "cold" subduction zones (e.g., Izu-Bonin) modeled by van Keken et al. (2011; after Syracuse et al., 2010).

4.2.3. Time-Dependent Variation of Wedge Hydration

We next compare the amount of H_2O delivered to the forearc wedge (Figures 8 and 9) with the H_2O capacity of the wedge (Figure 7; Figure S6 in Supporting Information S1) to arrive at the modeled estimates for wedge hydration ratio through time. As shown in Figure 7, the wedge H_2O capacity increases with continued subduction. During the early subduction phase (slow and hot) all modeled slabs contribute near equivalent cumulative amounts of H_2O to the wedge, after which the sediment-bearing models begin to have a higher H_2O contribution (yellow dashed lines in Figures 10a and 10b). By dividing the cumulative mass of H_2O delivered to the forearc by the wedge H_2O capacity, we can estimate the hydration ratio through time (relative amount of mantle wedge hydration as a percentage of its H_2O capacity; gray bars in Figures 10a and 10b, right axis). For the weak crust cases, the hydration ratio is initially low but increases to a maximum of 60%–70% during the intermediate phase before again decreasing to near constant values of 32% and 42% at 40 Myr for the Wn and Ws cases, respectively. This increase and then decrease in hydration ratio is a result of competition between H_2O fluid supplied from the

EPSTEIN ET AL. 14 of 27

2576604x, 2024, 4, Downloaded from https://agupubs.onlinelibrary.wiley.com/doi/10.1029/2023AV001121 by University Of Miami Libraries, Wiley Online Library on [2607/2024]. See the Terms

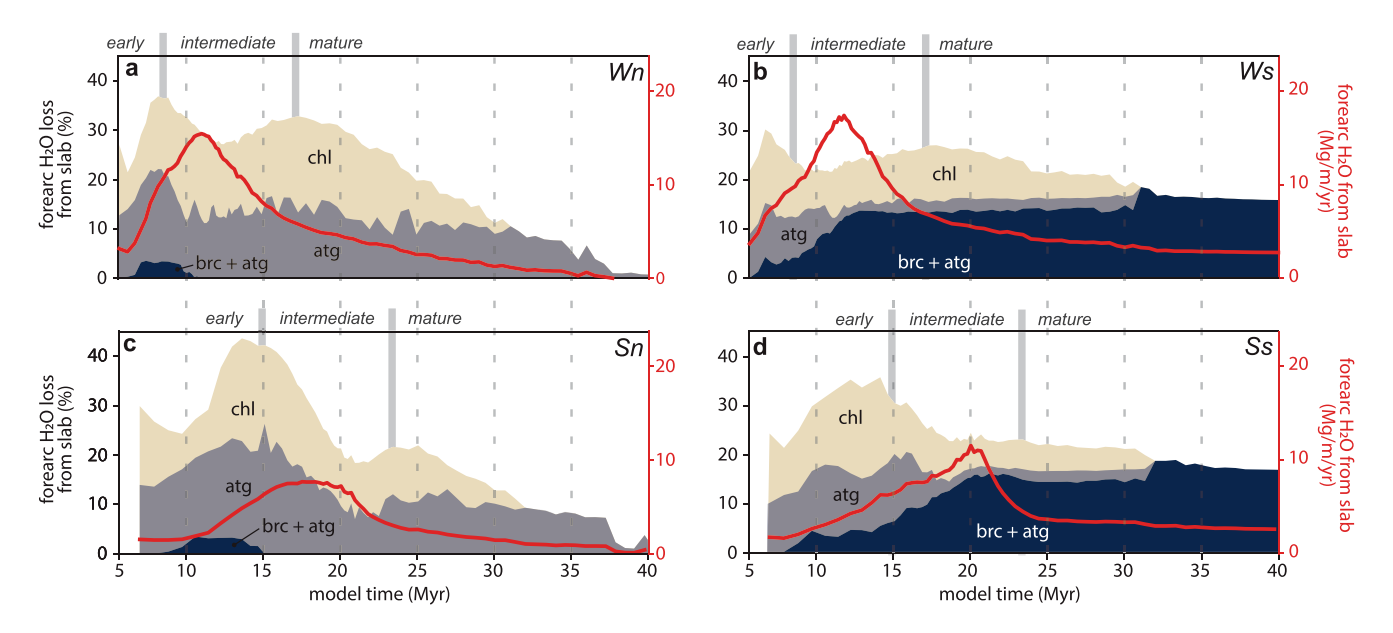


Figure 9. Forearc dehydration systematics as a function of fractional loss of H_2O from the downgoing slab (shaded regions) and as net mass of fluid released (red lines, right axis) for all model cases. (a, b) Weak crustal cases; (c, d) strong crustal cases. Shaded regions correspond to cumulative fluid loss from slab into the three hydrous mineral assemblages stable in the forearc wedge as a percent of fluid initially bound in the slab. Labels correspond to brucite + antigorite, antigorite (+olivine), and chlorite (+olivine + orthopyroxene). Colors correspond to Figure 6. For all cases maximum forearc slab dehydration occurs during the intermediate phase. Brucite-stable assemblages are only significant for the sediment-bearing cases.

slab and the increased wedge H_2O capacity due to cooling in the forearc. The rate of H_2O fluid supply from the slab initially outpaces the rate of mantle wedge H_2O capacity growth, but as convergence rates decrease and dehydration dominantly shifts to subarc depths, the H_2O capacity growth rate outpaces the rate of fluid supply (vertical dashed line in Figure 10). In the strong crust cases, both the total H_2O capacity of the wedge and H_2O contributions from the slab are less than for the weak crust model with maximum values for wedge hydration of $\sim 30\%$ and 38% during the intermediate phase and near constant values of 22% and 32% at 40 Myr for the Sn and Ss cases, respectively.

5. Discussion

5.1. Primary and Secondary Controls on Mantle Wedge Hydration

Our analysis suggests that the most pronounced wedge hydration occurs during the intermediate subduction phase, when slab velocities are high, and dehydration has not yet progressed to beyond forearc depths (Figures 8 and 10). Importantly, this geodynamic progression—from slow early subduction to rapid free sinking and then back to slower subduction as the slab interacts with stronger lower mantle—is observed in many dynamic subduction models that incorporate a 660 km mantle viscosity contrast, regardless of how the slab interacts with the contrast (e.g., Billen, 2008; Enns et al., 2005; Garel et al., 2014). Thus, while the discussion below focuses on results of the present study, the main points are highlighted in a broader context applicable to general subduction processes.

5.1.1. Modeling and Observation of Slab and Forearc Thermal Structure Variation

The timing and absolute magnitudes of slab dehydration and wedge hydration varies between our models, but they all demonstrate a broadly similar evolution (Figures 4, 5, and 9): in all cases the most pronounced addition of H_2O to the forearc mantle wedge occurs during the intermediate subduction phase when convergence rates are high and the onset of slab dehydration occurs beneath a relatively cool mantle wedge ($<\sim750^{\circ}C$; Figures 2 and 9). The interaction of two dynamic factors produces the most wedge hydration during this period: (a) the depth and magnitude of slab dehydration; and (b) the thermal state of the forearc wedge. These first order trends are observed irrespective of crustal strength or sediment availability, which only act to modify timing and absolute magnitudes, respectively.

EPSTEIN ET AL. 15 of 27

2576604x, 2024, 4, Downloaded from https://agupubs.on/inelibrary.wiley.com/doi/10.1029/2023AV001121 by University Of Mami Libraries, Wiley Online Library on [26/07/2024]. See the Terms and Conditions (https://onlinelibrary.wiley.com/terms-and-conditions) on Wiley Online Library or rules of use; OA articles

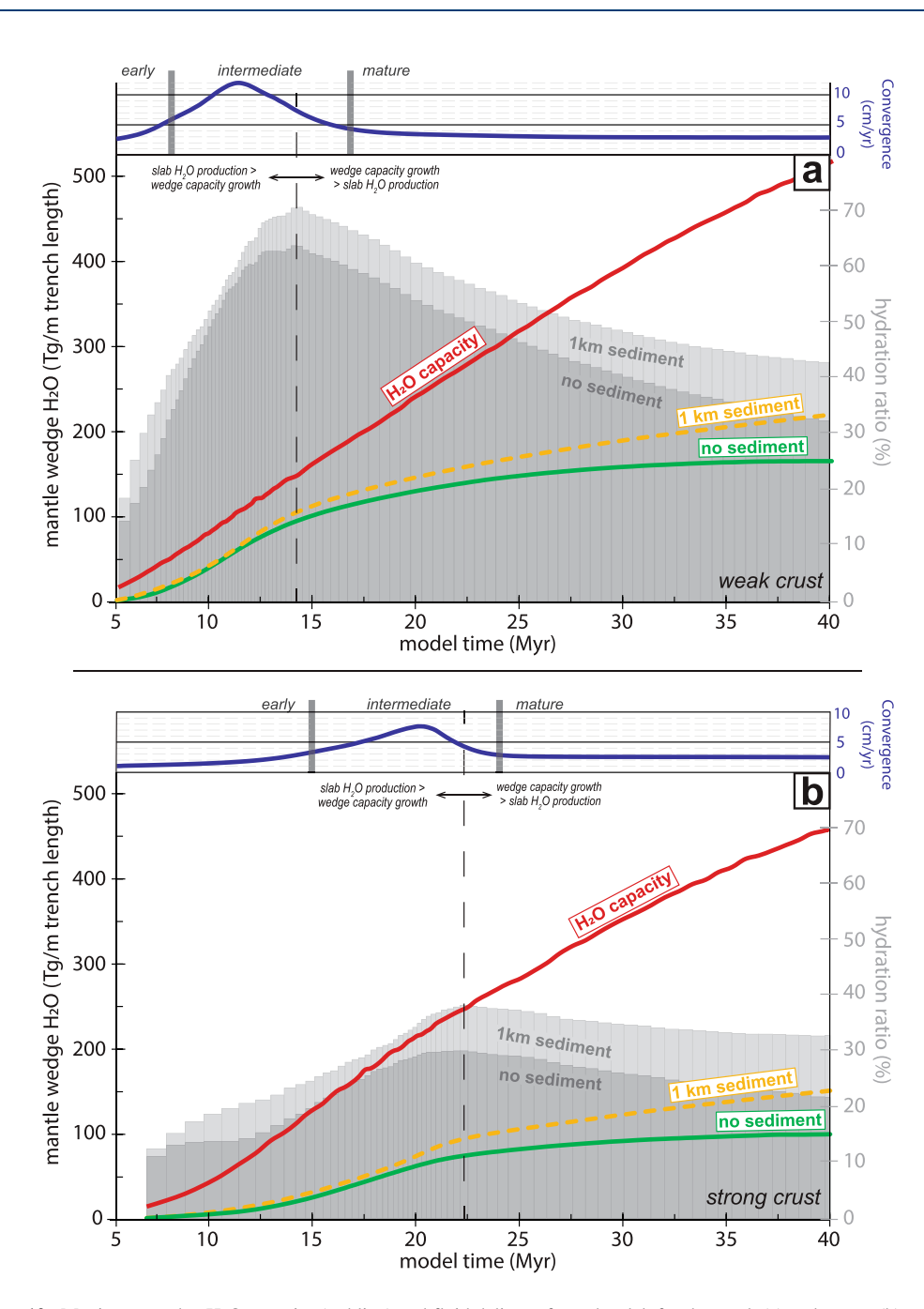


Figure 10. Maximum wedge H_2O capacity (red line) and fluid delivery from the slab for the weak (a) and strong (b) crustal cases (without sediment: green line; with sediment: yellow dashed line). Gray bars correspond to mantle wedge hydration ratio (%, right axis), indicating maximum hydration during the intermediate phase. The quasi steady state hydration ratios range from 22% to 42% at 40 Myr.

During early subduction, the warm and slowly subducting slab is completely dehydrated at shallow depths but the forearc wedge is too hot to stabilize large volumes of hydrous minerals (Figures 2a, 8, and 10). A hot, nominally anhydrous, forearc mantle wedge during incipient and early subduction has been inferred from geochemical and spatial variations across volcanic arcs and is consistent with our results. For example, boninites, which are high-Mg andesites derived from primary hydrous melting of a peridotite source at pressures of less than $<\sim$ 2 GPa (60 km) and temperatures in excess of 1,200°C, are found almost exclusively in forearc settings and are erupted during the early stages of subduction (Cluzel et al., 2016; Crawford et al., 1989; Hickey & Frey, 1982). A similar line of evidence comes from the observation of ancient near trench magmatism in regions that today have below

EPSTEIN ET AL. 16 of 27

average heat flow (Stern & Bloomer, 1992), suggesting that the forearc was warm enough to promote mantle melting earlier in the subduction cycle.

The intermediate period of subduction is characterized by rapid slab sinking (high convergence rates) through the upper mantle. This results in somewhat counterintuitive behavior: the slab interior is cold, but the slab top is rapidly heated below the forearc corner leading to the very large thermal gradients within the subducting slab (Figure 2d). Because the upper few km of the slab are still hot while the forearc is undergoing cooling, there is a large net flux of aqueous fluid into the forearc from the slab. Present day examples of this intermediate phase are rare, perhaps occurring within the southern section of the Vanuatu/New Hebrides subduction segment (age ~15 Myr) where the slab demonstrates high dip, rapid convergence (12.5 cm/yr), and considerable rollback (DeMets et al., 2010; Hall & Spakman, 2002; Schellart et al., 2006). Evidence for elevated convergence rates during this intermediate, slab sinking phase has been identified, for example, in the Mediterranean (Faccenna et al., 2001), and has been proposed for Izu-Bonin Marianas and Jurassic subduction offshore of California (Stern & Bloomer, 1992). Such elevated slab sinking rates during the intermediate subduction phase, with a subsequent slow down as the slab hits the more viscous lower mantle, are also commonly found within other subduction modeling studies (e.g., Enns et al., 2005; Garel et al., 2014; Holt et al., 2015; S. Zhong & Gurnis, 1995).

This convergence rate reduction, as the slab tip interacts and lays flat on top of, or penetrates, the upper-to-lower mantle viscosity increase at a depth of 660 km, leads to a decrease in thermal gradients within the slab (i.e., the interior of the slab becomes warmer than previous timesteps; Figures 2c and 2d). The change in velocity and slab thermal structure results in a transition between the intermediate phase (fast convergence and thin-skinned slab heating) and the mature or quasi-steady state phase (slower convergence with more extensive slab heating shifted to greater depths; Figure 4). This ultimately causes slab dehydration (mainly from basalts) to shift beyond depths where hydrous minerals are stable within the wedge (>80 km).

As the non-sediment cases (*Sn* and *Wn*) approach quasi-steady state conditions, forearc aqueous fluid release from the slab becomes negligible, consistent with results for "cold" subduction zones modeled using kinematically driven models (e.g., Sunda & Izu-Bonin Marianas, margins of Abers et al., 2017; red lines in Figures 9a and 9b). The sediment-bearing cases (*Ss* and *Ws*) on the other hand indicate a small contribution of slab aqueous fluids to the forearc at the end of the models (Figures 9c and 9d). Most of Earth's subduction systems appear to reside within this mature subduction phase, as is supported by observations of arc locations (England et al., 2004; Syracuse & Abers, 2006), tomographic images showing most slabs either flattening on top of or penetrating into the lower mantle (e.g., C. Li et al., 2008; Simmons et al., 2012), and the matching of geochemical proxies to kinematically driven models of steady-state subduction (e.g., Plank et al., 2009).

5.1.2. Influence of Crustal Strength and Volatile Supply on Hydration Timing and Magnitude

We have generalized our model results by examining the impact of variable (a) crustal strengths and (b) composition of the downgoing material on the timing and extent of wedge hydration. A stronger crust increases the subduction-resisting shear stresses and, in turn, reduces convergence rates (Behr & Becker, 2018; Conrad & Hager, 1999). Such slower convergence ultimately leads to slightly less cooling of the mantle wedge and delayed timings in the main subduction phases. Models with a stronger crust (*Sn*, *Ss*) experience delayed and decreased aqueous fluid release relative to models with a weaker crust (Figures 5 and 10). However, overall, the variation introduced by changing crustal strength does not drastically alter the hydrous mantle wedge mineralogy (Figure 9), nor does it produce a major difference in the magnitude of aqueous fluid release as the models approach steady state (cf. Figures 10a and 10b).

Variation in the composition and hydration state of subducted lithologies further modifies the magnitude of wedge hydration (Figures 4, 5, and 9). Greater amounts of sediment, or greater hydration of sediment, leads to more extensive H_2O transfer to the forearc mantle. The inclusion of a 1 km thick pelagic sedimentary section leads to an overall increase in wedge hydration of ~10% at 40 Myr for both crustal strengths (Figure 10). Thus, taken alone, sediment subduction exerts a secondary effect on wedge hydration ratio relative to the time-dependent thermal evolution of the slab and mantle wedge. In addition to sediment, the hydration state of the basalts and underlying materials may also contribute to variations in aqueous fluid supply to the wedge. For "typical" crustal sections, as tested here, gabbro and partially serpentinized peridotite do not contribute to forearc hydration (Figure 4), instead contributing to subarc or deeper mantle hydration. However, in the case of slow-spreading

EPSTEIN ET AL. 17 of 27

crust, oceanic core complex formation, or hydrated transform fault subduction, dehydration of these lithologies may also become important (e.g., Boschi et al., 2006; Paulatto et al., 2017; Wada et al., 2012).

Partially serpentinized peridotite below the Moho of the downgoing plate will only contribute to forearc wedge hydration in restricted cases. In thermal models, temperatures will always be higher above the subduction interface than within the crust and upper mantle below the interface. Thus, if temperatures are sufficient for serpentine dehydration within the downgoing slab, the forearc will be too warm to stabilize serpentine above the interface. There are three exceptions to this rule: first, dehydration across the brucite-out reaction within slab serpentinites (\sim 450°C) may be able to stabilize antigorite + olivine in the wedge (stable to \sim 625°C; Figure 6). Second, interface-parallel fluid flow could transport fluids from deeper along the interface into regions where hydrous phases are stable (Seno, 2005; Wilson et al., 2014). Third, the hydrated oceanic lithospheric mantle of the downgoing slab could dehydrate due to bottom-up heating (Arnulf et al., 2022; Cordell et al., 2023). These last two processes are not accounted for in the present model and would lead to higher degrees of hydration than inferred in the present work. We likewise do not observe any aqueous fluid release associated with low-T polymorphic reactions within the partially serpentinized lithospheric mantle of the downgoing slab because we assume hydration of ~15% (2 wt.% H₂O), which produces an assemblage where brucite is not stable. The hydration state of the incoming plate, as implemented in our models, is somewhat conservative (column average water contents of \sim 1.5 and \sim 2.1 wt.% for the non-sediment and sediment cases, respectively, Figure 3). Despite these relatively low values, the models predict extensive wedge hydration. Increasing the water content of the slab would likely serve to further increase magnitudes of mantle wedge hydration. Thus, the absolute magnitudes presented in our models (Table 1) represent minimum aqueous fluid production extents.

Our analysis—which factors in changing thermal state, subducting crustal strength variations, and variations in sediment supply—appears to capture first order dynamic processes that control wedge hydration despite there being a number of aspects we have not modeled, including varying the hydration state of the downgoing igneous crustal section (Jarrard, 2003), tectonic processes occurring in the overlying plate (e.g., backarc spreading; Kerswell et al., 2021), and flow of hydrated mantle material out of the forearc wedge (Honda et al., 2010; Nagaya et al., 2016). Based on the results of our dynamic approach, we propose that the primary control on extents of wedge hydration can be attributed to the non-steady state thermal conditions during the early and intermediate phases of subduction evolution.

Mantle wedge hydration is favored when the wedge has undergone considerable cooling and slab dehydration has not yet assumed its steady state distribution. In our models, maximum hydration ratios occur during the intermediate phase as the leading edge of the slab begins interacting with the 660 km mantle discontinuity and convergence rates begin decreasing but dehydration of the upper hydrated basalt section is still occurring within the forearc. A weaker slab, subducted sediments, or more extensive hydration of the oceanic crust will promote further wedge hydration but are secondary to the dynamic thermal evolution of the slab and wedge.

5.2. Comparison to Time-Invariant Thermal Models

Time-invariant kinematically driven thermal models predict a characteristic slab dehydration pattern with depth consisting of two main peaks associated with dehydration of igneous crust and hydrated lithospheric mantle. The shallower pulse of slab-derived H_2O occurs at or near the MDD ($\pm\sim10$ km; Epstein et al., 2021; Gorman et al., 2006; J. L. Li et al., 2020; van Keken et al., 2011; X. Zhong & Galvez, 2022), except for very young subducting slabs where it occurs in the shallower forearc (e.g., Cascadia, Mexico). The deeper pulse is associated with gabbro and partially serpentinized peridotite, and typically occurs at slabtop depths $\geq\sim120$ km. Previous slab dehydration and/or wedge hydration estimates made using time-invariant kinematically driven thermal models have examined variable slab ages (Gao & Wang, 2014; Syracuse et al., 2010; van Keken et al., 2011), sediment thicknesses and compositions (Hacker, 2008; van Keken et al., 2011), and H_2O and K_2O contents of the uppermost basalt sections (Jarrard, 2003). Most closely aligned with the present study, Abers et al. (2017) used the Syracuse et al. (2010) kinematically driven slab thermal structures to estimate the H_2O capacity of the mantle wedge for 56 segments of Earth's subduction system. By merging this result with phase equilibria modeling (from van Keken et al., 2011), Abers et al. (2017) predicted extents of wedge hydration occurring over 50 Myr for each segment.

We couple the slab dehydration estimates from our dynamic models with Abers et al.'s (2017) compiled mantle wedge H_2O capacities to compare predictions between dynamic and kinematically driven modeling approaches

EPSTEIN ET AL. 18 of 27

2576604x, 2024, 4, Downloaded from https://agupubs.onlinelibrary.wiley.com/doi/10.1029/2023AV001121 by University Of Miami Libraries, Wiley Online Library on [26/07/2024]. See the Terms

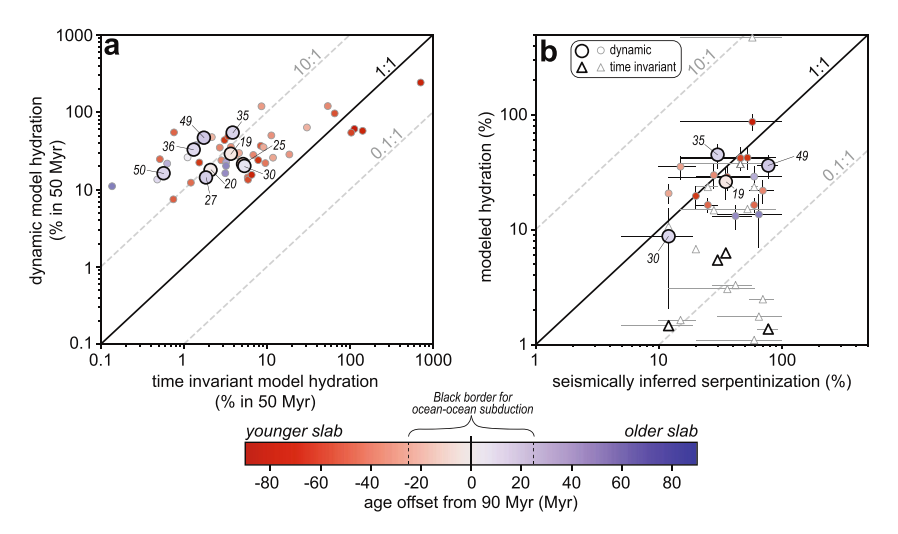


Figure 11. Comparison of mantle wedge hydration between time invariant and dynamic thermal models and comparison to seismically inferred serpentinization extents. (a) Comparison of modeled extents of forearc wedge hydration for time invariant models and the weak crustal case dynamic results. Sediment thickness and composition subducted for each data point, as well as kinematically driven hydration extents are taken from van Keken et al. (2011) and Abers et al. (2017), respectively. (b): Comparison between seismically inferred serpentinization extents and model results for time invariant models (open triangles) and dynamic model (filled circles). Error bars on filled circles on the *y*-axis represent the range between strong and weak crust models. Error bars on the *x*-axis represent the range of published serpentinization extents. Larger filled circles with black outline represent ocean-ocean subduction margins with downgoing plate ages of 90 ± 25 Myr. The dynamic model indicates ~1 order of magnitude greater hydration, and better agreement with seismic observation than kinematically driven models Labels after Abers et al. (2017): 19: N. Antilles; 20: S. Antilles; 25: S. Sumatra; 27: Java; 30: E. Banda Sea; 35: Tonga; 36: Kermadec; 49:Hokkaido; 50: S. Kurile.

(Figure 11a). In an effort to match each margin as closely as our models allow, we repeat the slab dehydration procedure outlined in the methods section while varying the subducted sediment thickness and composition to match those used in van Keken et al. (2011), modeling 0-1 km of subducted sediment with one of five different bulk compositions (pelagic, terrigenous, diatomaceous ooze, turbidite, and carbonate; see Table S2, Figures S7–S10 in Supporting Information S1). We do not vary the age of the downgoing plate (90 Myr), the hydration state of altered basalt (Figure 3), nor have we tailored convergence rates, slab dips, or overriding plate properties. We further make the simplifying assumption that all the modeled margins have undergone the same thermal evolution as detailed in Holt and Condit (2021). We focus our discussion on a subset of margins that broadly match our model assumptions: ocean-ocean subduction zones with downgoing plate ages of 90 ± 25 Myr.

Incorporation of early subduction evolution into wedge hydration calculations leads to an increase in hydration estimates for all but the youngest subducting plates (Figure 11a). Restricting our analysis to those margins with parameters most similar to that in our models we find that incorporating pre-steady state subduction leads to ~1 order of magnitude increase in hydration ratios over a 50 Myr period (larger points with black borders in Figure 11a). This increase is not dramatically different between the weak and strong crust cases, though the offset is somewhat less for the strong crust case (Figure S11 in Supporting Information S1). This comparison highlights the central importance of thermal evolution in stabilizing hydrous minerals in the mantle wedge. Because we have not incorporated geographic complexities, varied the age of the downgoing slab or tailored parameters beyond sediment type and thickness for each margin, the comparison to very young or very old subducting plates serves only to reveal the first-order trend.

5.3. Comparison to Geophysical Observations

Geophysical observation of a partially serpentinized mantle wedge is challenging. Seismic velocity perturbations are substantially smaller for the high temperature serpentine polymorph (antigorite) than for the lower T polymorphs (Bezacier et al., 2010; Birch, 1961; Ji et al., 2013), preferred crystallographic orientation of serpentine in the forearc may lead to very large variations in inferred extents due to anisotropies produced (Nagaya et al., 2016), and extrapolation of measured velocities over the entire mantle wedge requires numerous assumptions. With these caveats in mind, we have compiled estimates of serpentinization extents from the literature and compared

EPSTEIN ET AL. 19 of 27

them to results from our models presented here (both weak and strong crust cases, Figure 11b), again adopting the sediment thickness and composition outlined in van Keken et al. (2011). We have limited the geophysical compilation to studies that explicitly specify serpentinization extents as opposed to calculating extents; error bars are associated with the range of reported values, not actual measurement errors (see Abers et al., 2017 for a similar comparison). The dearth of sample points at low serpentinization extents is likely a sampling bias: investigations finding normal peridotite velocities do not calculate serpentinization extents. For this assessment we have extrapolated modeled hydration extents to the inferred age of the subduction zone by determining the aqueous fluid production from our models at quasi-steady state and extending those values to the inferred subduction age (ages after Schellart, 2020; see Supplementary Table 2 quasi-steady state fluid production estimates).

For margins where appreciable serpentinization is inferred (>10%), dynamic model results fall closer to a 1:1 correlation with observations (circles in Figure 11b), whereas kinematically driven models predict significantly less serpentinization than observationally estimated (open triangles in Figure 10b). The lack of a statistically robust correlation between observation and dynamic model results is likely due to the single age used in the present work for the downgoing slab but may also have contributions from the assumed lithologies being subducted, as well as the fact that unique subduction histories are not factored into the calculation. Despite such simplifications, this analysis highlights the significance of non-steady state thermal evolution in bringing dehydration models better in line with observations.

5.4. Implications for Rheology and Volatile Storage

In the present study, we estimate the overall hydration ratio of mantle wedges, rather than the spatial distribution of hydrous phases produced within the wedge. It is likely that the distribution of serpentine and other hydrous minerals will decrease with distance from the plate interface (Gerya et al., 2002; Hilairet & Reynard, 2009). Serpentine group minerals are much weaker than olivine, and only minor serpentinization (>~10%) is required to induce serpentine-like rheologies (Burdette & Hirth, 2022; Escartin et al., 2001). Geodynamic models of subduction require a weak boundary between the downgoing and overriding plates at depths less than the decoupling depth, with this weakening often hypothesized to be associated with serpentine or other hydrous phases (Hirauchi & Katayama, 2013; Peacock & Wang, 2021; Wada et al., 2008).

Early hydration associated with evolving thermal conditions is likely to stabilize a zone of hydration parallel to the plate interface and thus promote sustained subduction (so-called slabitization of Agard et al., 2020; Soret et al., 2022). Our minimum estimate of hydration ratios, from our strong crust case, predict that 42 of the 56 modeled subduction zones contain more than 10% wedge hydration (Supplementary Table 2, Figure S12 in Supporting Information S1), and thus would contain a rheologically weak mantle wedge. Likewise, of the 9 margins with similar plate ages and geodynamic settings, 7 contain more than 10% hydration. While we cannot speak to the processes that initiate subduction, our model provides a mechanism by which subduction can progress more easily as continued hydration occurs: the progressive increase in extents of serpentinization and in the depths of serpentine stability along or just above the plate interface (i.e., increasing depth of the DD; Guillot et al., 2015; Wada et al., 2008).

The hydrated forearc mantle wedge represents a significant global volatile reservoir, and aqueous fluids contained within wedges have been invoked in contributing to geodynamics of faulting (Kirby et al., 2014), orogeny (Humphreys et al., 2003), uplift (Porter et al., 2017), and post-collisional magmatism (Farmer et al., 2008). Our calculations suggest that every margin has some degree of hydration (minimum of 0.9%–5.3% for the Philippines; average of all models 18%–32%; for strong and weak crustal models, respectively). Considering along-strike subduction margin length (as compiled by van Keken et al., 2011) and applying the results of the present study, we estimate that the forearc mantle wedge may hold as much as 3.4– 5.9×10^{21} g H_2O ($\sim 0.25\%$ –0.4% of the present ocean mass; Sarmiento, 2006), leading to average global forearc wedge hydration ratios of 14%–23%.

Though the absolute values of slab dehydration and mantle wedge hydration ratios predicted by our models apply to the present model setup, the same progression of *relative changes* in convergence rate, slab dip, and slab thermal structure through time is observed in many models of subduction and are likely to promote mantle wedge hydration (Figure 12). We therefore posit that the relative changes in slab dehydration and mantle wedge hydration extent through time as observed in our models may be a common feature of subduction zone evolution globally.

EPSTEIN ET AL. 20 of 27

2576604x, 2024, 4, Downloaded from https://agupubs.onlinelibrary.wiley.com/doi/10.1029/2023AV001121 by University Of Miami Libraries, Wiley Online Library on [26/07/2024]. See the Terms and Conditions (https://onlinelibrary

com/terms-and-conditions) on Wiley Online Library for rules

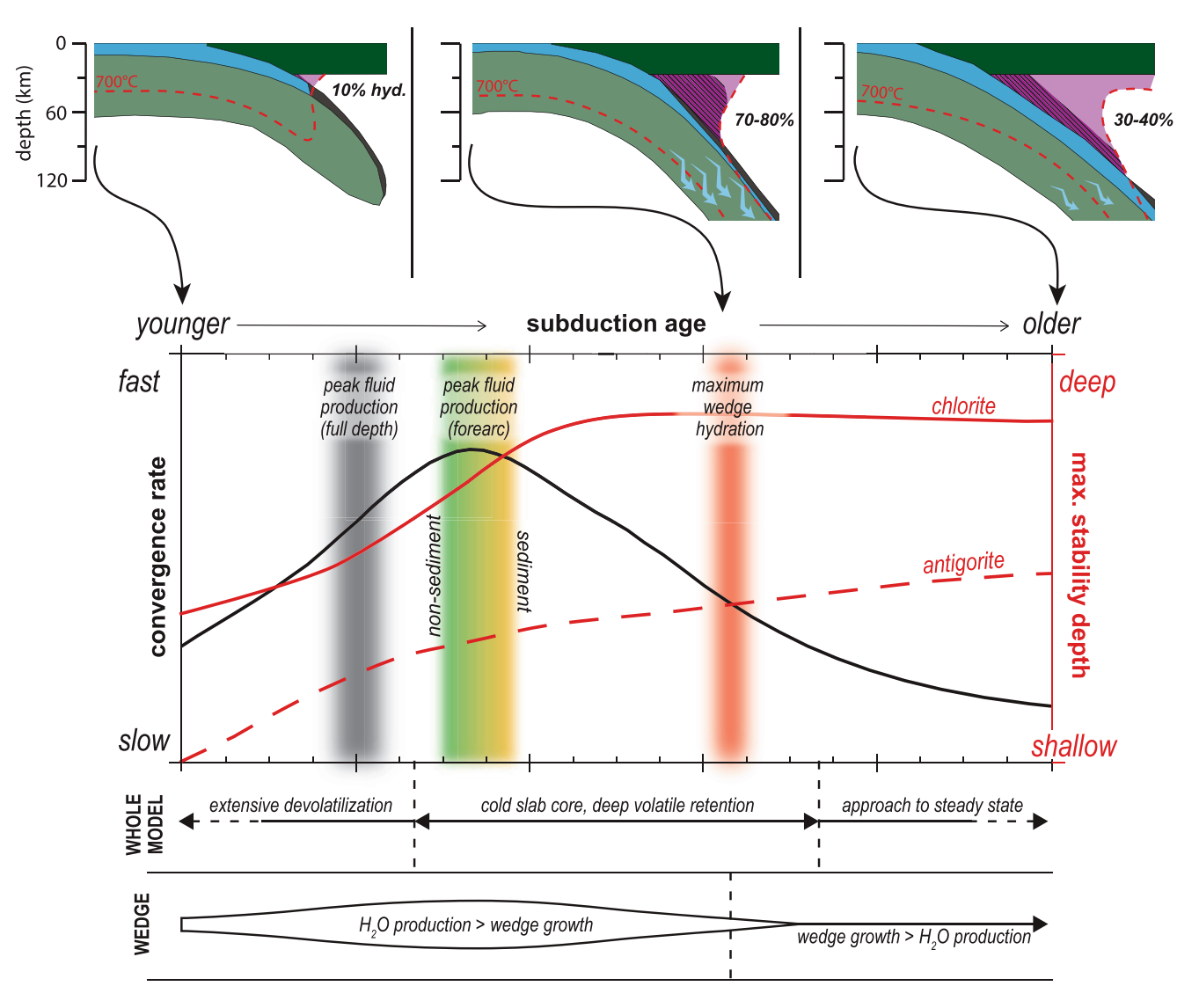


Figure 12. Summary of qualitative predictions of forearc wedge hydration during non-steady state subduction. During the early subduction stage the slab undergoes complete dehydration but the forearc is too warm to stabilize hydrous phases: maximum dehydration of the slab occurs during this timeframe and wedge hydration steadily increases. During the intermediate phase convergence rates are high, and the forearc has the largest mass input of aqueous fluid from the slab even though the slab interior remains cold. During the mature phase the increase of wedge H₂O capacity outcompetes fluid availability, and hydration extents decrease as quasi-steady state conditions are approached.

6. Conclusions

We have modeled extents of forearc mantle wedge hydration by coupling subduction thermal fields predicted by dynamic and time-dependent subduction models with phase equilibria calculations. In all of our models, factoring in variable volatile inventories and crustal strengths, the thermal evolution throughout the lifetime of the subduction zone promotes extensive forearc mantle wedge hydration. Maximum hydration ratios occur during the intermediate phase of subduction (i.e., as the slab is sinking rapidly through the upper mantle) when forearc temperatures are cool enough to stabilize large volumes of hydrous minerals and slabtop conditions are still warm enough to liberate aqueous fluids within the forearc. The exact timing of this maximum is dependent on the strength of the downgoing crust via its effect on subduction zone convergence rate (stronger crust leads to slower subduction and so later maximum dehydration), and its magnitude is amplified by the presence of sediments. Though the absolute values of the magnitude and timing of slab dehydration and mantle wedge hydration extent are specific to the models presented here, the relative changes in slab thermal structure as a function of changes in

EPSTEIN ET AL. 21 of 27

com/doi/10.1029/2023AV001121 by University Of Miami

Wiley Online Library on [26/07/2024]. See

convergence rates through time—and thus the relative changes in slab dehydration and mantle wedge hydration through time—may be a common characteristic of subduction zone evolution globally.

Predictions from this dynamic modeling approach indicate about an order of magnitude greater hydration than that predicted by previous studies that adopt fixed geometry, steady state thermal models; this suggests that the early thermal evolution in subduction zones may be important for explaining geophysical and chemical systematics of many of Earth's subduction zones. These increased hydration estimates are broadly consistent with observational inferences of wedge serpentinization extents. Our findings suggest that mantle wedge hydration is likely to be present to some degree at all subduction margins. A first order calculation, not factoring in plate ages or other factors unique to individual margins, suggests a maximum value for H_2O bound in forearc mantle wedge environments to be $3.4–5.9\times10^{21}$ g globally.

Conflict of Interest

The authors declare no conflicts of interest relevant to this study.

Data Availability Statement

All software and datafiles are available in the wedge_serpentinization Zenodo repository (Epstein, 2024) available at: https://zenodo.org/records/11244822.

References

- Abe, Y., Ohkura, T., Hirahara, K., & Shibutani, T. (2013). Along-arc variation in water distribution in the uppermost mantle beneath Kyushu, Japan, as derived from receiver function analyses. *Journal of Geophysical Research: Solid Earth*, 118(7), 3540–3556. https://doi.org/10.1002/jorb.50257
- Abers, G. A., Van Keken, P. E., & Hacker, B. R. (2017). The cold and relatively dry nature of mantle forearcs in subduction zones. *Nature Geoscience*, 10(5), 333–337, https://doi.org/10.1038/ngeo2922
- Agard, P., Prigent, C., Soret, M., Dubacq, B., Guillot, S., & Deldicque, D. (2020). Slabitization: Mechanisms controlling subduction development and viscous coupling. Earth-Science Reviews, 208, 103259. https://doi.org/10.1016/j.earscirev.2020.103259
- Agard, P., Yamato, P., Jolivet, L., & Burov, E. (2009). Exhumation of oceanic blueschists and eclogites in subduction zones: Timing and mechanisms. *Earth-Science Reviews*, 92(1–2), 53–79. https://doi.org/10.1016/j.earscirev.2008.11.002
- Agrusta, R., Goes, S., & Van Hunen, J. (2017). Subducting-slab transition-zone interaction: Stagnation, penetration and mode switches. *Earth and Planetary Science Letters*, 464, 10–23. https://doi.org/10.1016/j.epsl.2017.02.005
- Arcay, D., Tric, E., & Doin, M.-P. (2005). Numerical simulations of subduction zones: Effect of slab dehydration on the mantle wedge dynamics. *Physics of the Earth and Planetary Interiors*, 149(1–2), 133–153. https://doi.org/10.1016/j.pepi.2004.08.020
- Arnulf, A. F., Bassett, D., Harding, A. J., Kodaira, S., Nakanishi, A., & Moore, G. (2022). Upper-plate controls on subduction zone geometry, hydration and earthquake behaviour. *Nature Geoscience*, 15(2), 143–148. https://doi.org/10.1038/s41561-021-00879-x
- Bangerth, W., Dannberg, J., Gassmoeller, R., & Heister, T. (2020a). ASPECT v2.1.0. Zenodo. https://doi.org/10.5281/ZENODO.3924604
 Bangerth, W., Dannberg, J., Gassmoeller, R., & Heister, T. (2020b). ASPECT: Advanced solver for problems in Earth's convection. User Manual. https://doi.org/10.6084/m9.figshare.4865333
- Beaumont, C., Ellis, S., & Pfiffner, A. (1999). Dynamics of sediment subduction-accretion at convergent margins: Short-term modes, long-term deformation, and tectonic implications. *Journal of Geophysical Research*, 104(B8), 17573–17601. https://doi.org/10.1029/1999jb900136
- Behr, W. M., & Becker, T. W. (2018). Sediment control on subduction plate speeds. Earth and Planetary Science Letters, 502, 166–173. https://doi.org/10.1016/j.epsl.2018.08.057
- Behr, W. M., Holt, A. F., Becker, T. W., & Faccenna, C. (2022). The effects of plate interface rheology on subduction kinematics and dynamics. Geophysical Journal International, 230(2), 796–812. https://doi.org/10.1093/gji/ggac075
- Bezacier, L., Reynard, B., Bass, J. D., Sanchez-Valle, C., & Van de Moortèle, B. (2010). Elasticity of antigorite, seismic detection of serpentinites, and anisotropy in subduction zones. *Earth and Planetary Science Letters*, 289(1–2), 198–208. https://doi.org/10.1016/j.epsl.2009.11.009
 Billen, M. I. (2008). Modeling the dynamics of subducting slabs. *Annual Review of Earth and Planetary Sciences*, 36(1), 325–356. https://doi.org/
- Billen, M. I. (2008). Modeling the dynamics of subducting slabs. *Annual Review of Earth and Planetary Sciences*, 36(1), 325–356. https://doi.org/10.1146/annurev.earth.36.031207.124129
- Birch, F. (1961). The velocity of compressional waves in rocks to 10 kilobars, Part 2. Journal of Geophysical Research, 66(7), 2199–2224. https://doi.org/10.1029/jz066i007p02199
- Blakely, R. J., Brocher, T. M., & Wells, R. E. (2005). Subduction-zone magnetic anomalies and implications for hydrated forearc mantle. *Geology*, 33(6), 445–448. https://doi.org/10.1130/g21447.1
- Boschi, C., Früh-Green, G. L., Delacour, A., Karson, J. A., & Kelley, D. S. (2006). Mass transfer and fluid flow during detachment faulting and development of an oceanic core complex, Atlantis Massif (MAR 30 N). *Geochemistry, Geophysics, Geosystems*, 7(1), 1–39. https://doi.org/10.1029/2005gc001074
- Bostock, M. G., Hyndman, R. D., Rondenay, S., & Peacock, S. M. (2002). An inverted continental Moho and serpentinization of the forearc mantle. *Nature*, 417(6888), 536–538. https://doi.org/10.1038/417536a
- Bromiley, G. D., & Pawley, A. R. (2003). The stability of antigorite in the systems MgO-SiO₂-H₂O (MSH) and MgO-Al₂O₃-SiO₂-H₂O (MASH): The effects of Al³⁺ substitution on high-pressure stability. *American Mineralogist*, 88(1), 99–108. https://doi.org/10.2138/am-2003-0113
- Burdette, E., & Hirth, G. (2022). Creep rheology of antigorite: Experiments at subduction zone conditions. *Journal of Geophysical Research:* Solid Earth, 127(7), e2022JB024260. https://doi.org/10.1029/2022jb024260
- Carlson, R. L., & Miller, D. J. (2003). Mantle wedge water contents estimated from seismic velocities in partially serpentinized peridotites. Geophysical Research Letters, 30(5), 1250. https://doi.org/10.1029/2002gl016600

Acknowledgments

We acknowledge support from the NSF EAR Geophysics and Petrology and Geochemistry Programs (awards 2119842, 2119843, and 2119844 awarded to AFH, VEG, and CBC, respectively). Colormaps are from the colorcet package (colorcet. com; Kovesi, 2015). Map figures were made in pygmt (Tian, 2023; Wessel et al., 2019). We are grateful for constructive comments from Kelin Wang, Andrés Tessara, and two anonymous reviewers that greatly improved this manuscript. We also thank Marcos Moreno for editorial handling and additional helpful comments.

EPSTEIN ET AL. 22 of 27

- Chen, Z., Chen, J., Zeng, Z., Soh Tamehe, L., Zhang, T., Zhang, Y., et al. (2021). Zinc isotopes of the Mariana and Ryukyu arc-related lavas reveal recycling of forearc serpentinites into the subarc mantle. *Journal of Geophysical Research: Solid Earth*, 126(11), e2021JB022261. https://doi.org/10.1029/2021jb022261
- Christensen, N. I. (1966). Elasticity of ultrabasic rocks. *Journal of Geophysical Research*, 71(24), 5921–5931. https://doi.org/10.1029/jz071i024p05921
- Čížková, H., & Bina, C. R. (2013). Effects of mantle and subduction-interface rheologies on slab stagnation and trench rollback. Earth and Planetary Science Letters, 379, 95–103. https://doi.org/10.1016/j.epsl.2013.08.011
- Cluzel, D., Ulrich, M., Jourdan, F., Meffre, S., Paquette, J. L., Audet, M. A., et al. (2016). Early Eocene clinoenstatite boninite and boninite-series dikes of the ophiolite of New Caledonia; a witness of slab-derived enrichment of the mantle wedge in a nascent volcanic arc. *Lithos*, 260, 429–442. https://doi.org/10.1016/j.lithos.2016.04.031
- Connolly, J. A. (2005). Computation of phase equilibria by linear programming: A tool for geodynamic modeling and its application to subduction zone decarbonation. *Earth and Planetary Science Letters*, 236(1–2), 524–541. https://doi.org/10.1016/j.epsl.2005.04.033
- Conrad, C. P., & Hager, B. H. (1999). Effects of plate bending and fault strength at subduction zones on plate dynamics. *Journal of Geophysical Research*, 104(B8), 17551–17571. https://doi.org/10.1029/1999jb900149
- Cordell, D., Naif, S., Evans, R., Key, K., Constable, S., Shillington, D., & Bécel, A. (2023). Forearc seismogenesis in a weakly coupled subduction zone influenced by slab mantle fluids. *Nature Geoscience*, 16(9), 1–6. https://doi.org/10.1038/s41561-023-01260-w
- Crawford, A. J., Falloon, T. J., & Green, D. H. (1989). Classification, petrogenesis and tectonic setting of boninites. In *Boninites and related rocks* (pp. 1–49).
- DeMets, C., Gordon, R. G., & Argus, D. F. (2010). Geologically current plate motions. *Geophysical Journal International*, 181(1), 1–80. https://doi.org/10.1111/j.1365-246x.2009.04491.x
- Deschamps, F., Godard, M., Guillot, S., & Hattori, K. (2013). Geochemistry of subduction zone serpentinites: A review. *Lithos*, 178, 96–127. https://doi.org/10.1016/j.lithos.2013.05.019
- DeShon, H. R., & Schwartz, S. Y. (2004). Evidence for serpentinization of the forearc mantle wedge along the Nicoya Peninsula, Costa Rica. Geophysical Research Letters, 31(21), L21611. https://doi.org/10.1029/2004g1021179
- Dick, H. J., Natland, J. H., Alt, J. C., Bach, W., Bideau, D., Gee, J. S., et al. (2000). A long in situ section of the lower ocean crust: Results of ODP Leg 176 drilling at the southwest Indian ridge. *Earth and Planetary Science Letters*, 179(1), 31–51. https://doi.org/10.1016/s0012-821x(00) 00102-3
- Doo, W. B., Kuo-Chen, H., Brown, D., Lo, C. L., Hsu, S. K., & Huang, Y. S. (2016). Serpentinization of the fore-arc mantle along the Taiwan arccontinent collision of the northern Manila subduction zone inferred from gravity modeling. *Tectonophysics*, 691, 282–289. https://doi.org/10. 1016/j.tecto.2016.10.019
- England, P., Engdahl, R., & Thatcher, W. (2004). Systematic variation in the depths of slabs beneath arc volcanoes. *Geophysical Journal International*, 156(2), 377–408. https://doi.org/10.1111/j.1365-246x.2003.02132.x
- Enns, A., Becker, T. W., & Schmeling, H. (2005). The dynamics of subduction and trench migration for viscosity stratification. *Geophysical Journal International*, 160(2), 761–775. https://doi.org/10.1111/j.1365-246x.2005.02519.x
- Epstein, G. (2024). wedge_serpentinization (v1.0.0). Zenodo. https://doi.org/10.5281/zenodo.11244822
- Epstein, G. S., Bebout, G. E., Christenson, B. W., Sumino, H., Wada, I., Werner, C., & Hilton, D. R. (2021). Cycling of CO₂ and N₂ along the Hikurangi Subduction Margin, New Zealand: An integrated geological, theoretical, and isotopic approach. *Geochemistry, Geophysics, Geosystems*, 22(9), e2021GC009650. https://doi.org/10.1029/2021gc009650
- Ernst, W. G. (2005). Alpine and Pacific styles of phanerozoic mountain building: Subduction-zone petrogenesis of continental crust. *Terra Nova*, 17(2), 165–188. https://doi.org/10.1111/j.1365-3121.2005.00604.x
- Escartin, J., Hirth, G., & Evans, B. (2001). Strength of slightly serpentinized peridotites: Implications for the tectonics of oceanic lithosphere. Geology, 29(11), 1023–1026. https://doi.org/10.1130/0091-7613(2001)029<1023:sosspi>2.0.co;2
- Evans, B. W. (2008). Control of the products of serpentinization by the Fe²⁺ Mg₋₁ exchange potential of olivine and orthopyroxene. *Journal of Petrology*, 49(10), 1873–1887. https://doi.org/10.1093/petrology/egn050
- Faccenna, C., Becker, T. W., Lucente, F. P., Jolivet, L., & Rossetti, F. (2001). History of subduction and back arc extension in the Central Mediterranean. *Geophysical Journal International*, 145(3), 809–820. https://doi.org/10.1046/j.0956-540x.2001.01435.x
- Farmer, G. L., Bailley, T., & Elkins-Tanton, L. T. (2008). Mantle source volumes and the origin of the mid-Tertiary ignimbrite flare-up in the southern Rocky Mountains, western US. *Lithos*, 102(1–2), 279–294. https://doi.org/10.1016/j.lithos.2007.08.014
- Frost, B. R., & Beard, J. S. (2007). On silica activity and serpentinization. *Journal of Petrology*, 48(7), 1351–1368. https://doi.org/10.1093/petrology/egm021
- Furukawa, Y. (1993). Depth of the decoupling plate interface and thermal structure under arcs. *Journal of Geophysical Research*, 98(B11), 20005–20013. https://doi.org/10.1029/93jb02020
- Fyfe, W. S., & McBirney, A. R. (1975). Subduction and the structure of andesitic volcanic belts. American Journal of Science, 275(1), 285–297.
 Gale, A., Dalton, C. A., Langmuir, C. H., Su, Y., & Schilling, J. G. (2013). The mean composition of ocean ridge basalts. Geochemistry, Geophysics, Geosystems, 14(3), 489–518. https://doi.org/10.1029/2012gc004334
- Gao, X., & Wang, K. (2014). Strength of stick-slip and creeping subduction megathrusts from heat flow observations. Science, 345(6200), 1038–1041. https://doi.org/10.1126/science.1255487
- Garel, F., Goes, S., Davies, D. R., Davies, J. H., Kramer, S. C., & Wilson, C. R. (2014). Interaction of subducted slabs with the mantle transition-zone: A regime diagram from 2-D thermo-mechanical models with a mobile trench and an overriding plate. *Geochemistry, Geophysics, Geosystems*, 15(5), 1739–1765. https://doi.org/10.1002/2014gc005257
- Gerya, T. V., Stöckhert, B., & Perchuk, A. L. (2002). Exhumation of high-pressure metamorphic rocks in a subduction channel: A numerical simulation. Tectonics, 21(6), 6-1. https://doi.org/10.1029/2002tc001406
- Goes, S., Agrusta, R., van Hunen, J., & Garel, F. (2017). Subduction-transition zone interaction: A review. Geosphere, 13(3), 644–664. https://doi.org/10.1130/ges01476.1
- Gorman, P. J., Kerrick, D. M., & Connolly, J. A. D. (2006). Modeling open system metamorphic decarbonation of subducting slabs. Geochemistry, Geophysics, Geosystems, 7(4), Q04007. https://doi.org/10.1029/2005gc001125
- Guillot, S., Hattori, K. H., de Sigoyer, J., Nägler, T., & Auzende, A. L. (2001). Evidence of hydration of the mantle wedge and its role in the exhumation of eclogites. Earth and Planetary Science Letters, 193(1–2), 115–127. https://doi.org/10.1016/s0012-821x(01)00490-3
- Guillot, S., Schwartz, S., Reynard, B., Agard, P., & Prigent, C. (2015). Tectonic significance of serpentinites. *Tectonophysics*, 646, 1–19. https://doi.org/10.1016/j.tecto.2015.01.020
- Hacker, B. R. (2008). H₂O subduction beyond arcs. Geochemistry, Geophysics, Geosystems, 9(3), Q03001. https://doi.org/10.1029/2007gc001707

EPSTEIN ET AL. 23 of 27

- Hacker, B. R., Peacock, S. M., Abers, G. A., & Holloway, S. D. (2003). Subduction factory 2. Are intermediate-depth earthquakes in subducting slabs linked to metamorphic dehydration reactions? *Journal of Geophysical Research*, 108(B1), 2030. https://doi.org/10.1029/2001jb001129
 Hager, B. H. (1984). Subducted slabs and the geoid: Constraints on mantle rheology and flow. *Journal of Geophysical Research*, 89(B7), 6003–
- 6015. https://doi.org/10.1029/jb089ib07p06003
 Hall, P. S. (2012). On the thermal evolution of the mantle wedge at subduction zones. *Physics of the Earth and Planetary Interiors*, 198, 9–27. https://doi.org/10.1016/j.pepi.2012.03.004
- Hall, R., & Spakman, W. (2002). Subducted slabs beneath the eastern Indonesia—Tonga region: Insights from tomography. Earth and Planetary Science Letters, 201(2), 321–336. https://doi.org/10.1016/s0012-821x(02)00705-7
- Halpaap, F., Rondenay, S., Perrin, A., Goes, S., Ottemöller, L., Austrheim, H., et al. (2019). Earthquakes track subduction fluids from slab source to mantle wedge sink. *Science Advances*, 5(4), eaav7369. https://doi.org/10.1126/sciadv.aav7369
- Hattori, K. H., & Guillot, S. (2003). Volcanic fronts form as a consequence of serpentinite dehydration in the forearc mantle wedge. *Geology*, 31(6), 525–528. https://doi.org/10.1130/0091-7613(2003)031<0525:vffaac>2.0.co;2
- Heister, T., Dannberg, J., Gassmöller, R., & Bangerth, W. (2017). High accuracy mantle convection simulation through modern numerical methods—II: Realistic models and problems. *Geophysical Journal International*, 210(2), 833–851. https://doi.org/10.1093/gji/ggx195
- Hermann, J., Müntener, O., & Scambelluri, M. (2000). The importance of serpentinite mylonites for subduction and exhumation of oceanic crust. *Tectonophysics*, 327(3–4), 225–238. https://doi.org/10.1016/s0040-1951(00)00171-2
- Hickey, R. L., & Frey, F. A. (1982). Geochemical characteristics of boninite series volcanics: Implications for their source. Geochimica et Cosmochimica Acta, 46(11), 2099–2115. https://doi.org/10.1016/0016-7037(82)90188-0
- Hilairet, N., & Reynard, B. (2009). Stability and dynamics of serpentinite layer in subduction zone. *Tectonophysics*, 465(1–4), 24–29. https://doi.org/10.1016/j.tecto.2008.10.005
- Hirauchi, K. I., & Katayama, I. (2013). Rheological contrast between serpentine species and implications for slab–mantle wedge decoupling. *Tectonophysics*, 608, 545–551. https://doi.org/10.1016/j.tecto.2013.08.027
- Hirth, G., & Kohlstedt, D. (2003). Rheology of the upper mantle and the mantle wedge: A view from the experimentalists. In *Inside the subduction factory, geophysical monograph series 138* (pp. 83–105). https://doi.org/10.1029/138gm06
- Holland, T. J. B., & Powell, R. (2011). An improved and extended internally consistent thermodynamic dataset for phases of petrological interest, involving a new equation of state for solids. *Journal of Metamorphic Geology*, 29(3), 333–383. https://doi.org/10.1111/j.1525-1314.2010.
- Holt, A. F., Becker, T. W., & Buffett, B. A. (2015). Trench migration and overriding plate stress in dynamic subduction models. *Geophysical Journal International*, 201(1), 172–192. https://doi.org/10.1093/gji/ggv011
- Holt, A. F., & Condit, C. B. (2021). Slab temperature evolution over the lifetime of a subduction zone. *Geochemistry, Geophysics, Geosystems*, 22(6), e2020GC009476. https://doi.org/10.1029/2020gc009476
- Honda, S., Gerya, T., & Zhu, G. (2010). A simple three-dimensional model of thermo-chemical convection in the mantle wedge. *Earth and Planetary Science Letters*, 290(3–4), 311–318. https://doi.org/10.1016/j.epsl.2009.12.027
- Humphreys, E., Hessler, E., Dueker, K., Farmer, G. L., Erslev, E., & Atwater, T. (2003). How Laramide-age hydration of North American lithosphere by the Farallon slab controlled subsequent activity in the western United States. *International Geology Review*, 45(7), 575–595. https://doi.org/10.2747/0020-6814.45.7.575
- Hyndman, R. D., & Peacock, S. M. (2003). Serpentinization of the forearc mantle. Earth and Planetary Science Letters, 212(3-4), 417-432. https://doi.org/10.1016/s0012-821x(03)00263-2
- Jarrard, R. D. (2003). Subduction fluxes of water, carbon dioxide, chlorine, and potassium. Geochemistry, Geophysics, Geosystems, 4(5), 8905. https://doi.org/10.1029/2002gc000392
- Ji, S., Li, A., Wang, Q., Long, C., Wang, H., Marcotte, D., & Salisbury, M. (2013). Seismic velocities, anisotropy, and shear-wave splitting of antigorite serpentinites and tectonic implications for subduction zones. *Journal of Geophysical Research: Solid Earth*, 118(3), 1015–1037. https://doi.org/10.1002/jgrb.50110
- Karato, S.-I., & Wu, P. (1993). Rheology of the upper mantle: A synthesis. Science, 260(5109), 771–778. https://doi.org/10.1126/science.260. 5109.771
- Katayama, I., Hirauchi, K. I., Michibayashi, K., & Ando, J. I. (2009). Trench-parallel anisotropy produced by serpentine deformation in the hydrated mantle wedge. Nature, 461(7267), 1114–1117. https://doi.org/10.1038/nature08513
- Kerswell, B. C., Kohn, M. J., & Gerya, T. V. (2021). Backarc lithospheric thickness and serpentine stability control slab-mantle coupling depths in subduction zones. Geochemistry, Geophysics, Geosystems, 22(6), e2020GC009304. https://doi.org/10.1029/2020gc009304
- Kincaid, C., & Sacks, I. S. (1997). Thermal and dynamical evolution of the upper mantle in subduction zones. *Journal of Geophysical Research*, 102(B6), 12295–12315. https://doi.org/10.1029/96jb03553
- Kirby, S. H. (1995). Interslab earthquakes and phase changes in subducting lithosphere. *Reviews of Geophysics*, 33(S1), 287–297. https://doi.org/10.1029/95rg00353
- Kirby, S. H., Wang, K., & Brocher, T. M. (2014). A large mantle water source for the northern San Andreas fault system: A ghost of subduction past. Earth Planets and Space, 66, 1–18. https://doi.org/10.1186/1880-5981-66-67
- Kovesi, P. (2015). Good colour maps: How to design them. arXiv preprint arXiv:1509.03700.
- Kronbichler, M., Heister, T., & Bangerth, W. (2012). High accuracy mantle convection simulation through modern numerical methods. Geophysical Journal International, 191(1), 12–29. https://doi.org/10.1111/j.1365-246x.2012.05609.x
- Lee, C. T. A. (2005). Trace element evidence for hydrous metasomatism at the base of the North American lithosphere and possible association with Laramide low-angle subduction. *The Journal of Geology*, 113(6), 673–685. https://doi.org/10.1086/449327
- Li, C., van der Hilst, R. D., Engdahl, E. R., & Burdick, S. (2008). A new global model for P wave speed variations in Earth's mantle. *Geochemistry*, *Geophysics*, *Geosystems*, 9(5), Q05018. https://doi.org/10.1029/2007gc001806
- Li, C. F. (2011). An integrated geodynamic model of the Nankai subduction zone and neighboring regions from geophysical inversion and modeling. *Journal of Geodynamics*, 51(1), 64–80. https://doi.org/10.1016/j.jog.2010.08.003
- Li, J. L., Schwarzenbach, E. M., John, T., Ague, J. J., Huang, F., Gao, J., et al. (2020). Uncovering and quantifying the subduction zone sulfur cycle from the slab perspective. *Nature Communications*, 11(1), 514. https://doi.org/10.1038/s41467-019-14110-4
- Li, X., Bock, G., Vafidis, A., Kind, R., Harjes, H. P., Hanka, W., et al. (2003). Receiver function study of the Hellenic subduction zone: Imaging crustal thickness variations and the oceanic moho of the descending African lithosphere. *Geophysical Journal International*, 155(2), 733–748. https://doi.org/10.1046/j.1365-246x.2003.02100.x
- MacKenzie, L., Abers, G. A., Fischer, K. M., Syracuse, E. M., Protti, J. M., Gonzalez, V., & Strauch, W. (2008). Crustal structure along the southern Central American volcanic front. Geochemistry, Geophysics, Geosystems, 9(8), Q08S09. https://doi.org/10.1029/2008gc001991

EPSTEIN ET AL. 24 of 27

- Marsh, B. D. (1979). Island-Arc Volcanism: Volcanic arcs ringing the Pacific owe their origin to magma generated in a mysterious fashion when tectonic plates are consumed by the inner earth. *American Scientist*, 67, 161–172.
- Martin, C., Flores, K. E., Vitale-Brovarone, A., Angiboust, S., & Harlow, G. E. (2020). Deep mantle serpentinization in subduction zones: Insight from in situ B isotopes in slab and mantle wedge serpentinites. *Chemical Geology*, 545, 119637. https://doi.org/10.1016/j.chemgeo.2020. 119637
- Nagaya, T., Walker, A. M., Wookey, J., Wallis, S. R., Ishii, K., & Kendall, J. M. (2016). Seismic evidence for flow in the hydrated mantle wedge of the Ryukyu subduction zone. *Scientific Reports*, 6(1), 29981. https://doi.org/10.1038/srep29981
- Niu, Y. (2004). Bulk-rock major and trace element compositions of abyssal peridotites: Implications for mantle melting, melt extraction and post-melting processes beneath mid-ocean ridges. *Journal of Petrology*, 45(12), 2423–2458. https://doi.org/10.1093/petrology/egh068
- Oleskevich, D. A., Hyndman, R. D., & Wang, K. (1999). The updip and downdip limits to great subduction earthquakes: Thermal and structural models of Cascadia, South Alaska, SW Japan, and Chile. *Journal of Geophysical Research*, 104(B7), 14965–14991. https://doi.org/10.1029/1999jb900060
- Paulatto, M., Laigle, M., Galve, A., Charvis, P., Sapin, M., Bayrakci, G., et al. (2017). Dehydration of subducting slow-spread oceanic lithosphere in the Lesser Antilles. *Nature Communications*, 8(1), 15980. https://doi.org/10.1038/ncomms15980
- Peacock, S. M. (1996). Thermal and petrologic structure of subduction zones. In Subduction: Top to bottom (Vol. 96, pp. 119–133). https://doi.org/10.1029/gm096p0119
- Peacock, S. M., & Hyndman, R. D. (1999). Hydrous minerals in the mantle wedge and the maximum depth of subduction thrust earthquakes. Geophysical Research Letters, 26(16), 2517–2520. https://doi.org/10.1029/1999g1900558
- Peacock, S. M., & Wang, K. (1999). Seismic consequences of warm versus cool subduction metamorphism: Examples from southwest and northeast Japan. Science, 286(5441), 937–939. https://doi.org/10.1126/science.286.5441.937
- Peacock, S. M., & Wang, K. (2021). On the stability of talc in subduction zones: A possible control on the maximum depth of decoupling between the subducting plate and mantle wedge. *Geophysical Research Letters*, 48(17), e2021GL094889. https://doi.org/10.1029/2021gl094889
- Pitzer, K. S., & Sterner, S. M. (1994). Equations of state valid continuously from zero to extreme pressures for H₂O and CO₂. The Journal of Chemical Physics, 101(4), 3111–3116, https://doi.org/10.1063/1.467624
- Plank, T., Cooper, L. B., & Manning, C. E. (2009). Emerging geothermometers for estimating slab surface temperatures. *Nature Geoscience*, 2(9), 611–615. https://doi.org/10.1038/ngeo614
- Plank, T., & Langmuir, C. H. (1998). The chemical composition of subducting sediment and its consequences for the crust and mantle. *Chemical Geology*, 145(3–4), 325–394. https://doi.org/10.1016/s0009-2541(97)00150-2
- Porter, R., Hoisch, T., & Holt, W. E. (2017). The role of lower-crustal hydration in the tectonic evolution of the Colorado Plateau. *Tectonophysics*, 712, 221–231. https://doi.org/10.1016/j.tecto.2017.05.025
- Reynard, B., Mibe, K., & Van de Moortèle, B. (2011). Electrical conductivity of the serpentinised mantle and fluid flow in subduction zones. Earth and Planetary Science Letters, 307(3–4), 387–394. https://doi.org/10.1016/j.epsl.2011.05.013
- Sarmiento, J. L. (2006). Ocean biogeochemical dynamics (pp. 459-503). Princeton University Press.
- Schellart, W. P. (2020). Control of subduction zone age and size on flat slab subduction. Frontiers in Earth Science, 8, 26. https://doi.org/10.3389/
- Schellart, W. P., Lister, G. S., & Toy, V. G. (2006). A late Cretaceous and Cenozoic reconstruction of the southwest Pacific region: Tectonics controlled by subduction and slab rollback processes. *Earth-Science Reviews*, 76(3–4), 191–233. https://doi.org/10.1016/j.earscirev.2006. 01.002
- Schwartz, S., Allemand, P., & Guillot, S. (2001). Numerical model of the effect of serpentinites on the exhumation of eclogitic rocks: Insights from the Monviso ophiolitic massif (western Alps). *Tectonophysics*, 342(1–2), 193–206. https://doi.org/10.1016/s0040-1951(01)00162-7
- Seno, T. (2005). Variation of downdip limit of the seismogenic zone near the Japanese islands: Implications for the serpentinization mechanism of the forearc mantle wedge. Earth and Planetary Science Letters, 231(3-4), 249–262. https://doi.org/10.1016/j.epsl.2004.12.027
- Simmons, N. A., Myers, S. C., Johannesson, G., & Matzel, E. (2012). LLNL-G3Dv3: Global P wave tomography model for improved regional and teleseismic travel time prediction. *Journal of Geophysical Research*, 117(B10), 1–28. https://doi.org/10.1029/2012jb009525
- Sodoudi, F., Kind, R., Hatzfeld, D., Priestley, K., Hanka, W., Wylegalla, K., et al. (2006). Lithospheric structure of the Aegean obtained from P and S receiver functions. *Journal of Geophysical Research*, 111(B12), 218. https://doi.org/10.1029/2005jb003932
- Sodoudi, F., Yuan, X., Asch, G., & Kind, R. (2011). High-resolution image of the geometry and thickness of the subducting Nazca lithosphere beneath northern Chile. *Journal of Geophysical Research*, 116(B4), B04302. https://doi.org/10.1029/2010jb007829
- Soret, M., Bonnet, G., Agard, P., Larson, K. P., Cottle, J. M., Dubacq, B., et al. (2022). Timescales of subduction initiation and evolution of subduction thermal regimes. Earth and Planetary Science Letters, 584, 117521. https://doi.org/10.1016/j.epsl.2022.117521
- Stein, C. A., & Stein, S. (1992). A model for the global variation in oceanic depth and heat flow with lithospheric age. *Nature*, 359(6391), 123–129. https://doi.org/10.1038/359123a0
- Stern, R. J. (2004). Subduction initiation: Spontaneous and induced. Earth and Planetary Science Letters, 226(3-4), 275-292. https://doi.org/10.1016/j.epsl.2004.08.007
- Stern, R. J., & Bloomer, S. H. (1992). Subduction zone infancy: Examples from the Eocene Izu-Bonin-Mariana and Jurassic California arcs. Geological Society of America Bulletin, 104(12), 1621–1636. https://doi.org/10.1130/0016-7606(1992)104<1621:szieft>2.3.co;2
- Suenaga, N., Yoshioka, S., Matsumoto, T., Manea, V. C., Manea, M., & Ji, Y. (2019). Two-dimensional thermal modeling of the Philippine Sea plate subduction in central Japan: Implications for gap of low-frequency earthquakes and tectonic tremors. *Journal of Geophysical Research:* Solid Earth, 124(7), 6848–6865. https://doi.org/10.1029/2018jb017068
- Syracuse, E. M., & Abers, G. A. (2006). Global compilation of variations in slab depth beneath arc volcanoes and implications. *Geochemistry*, *Geophysics*, *Geosystems*, 7(5), Q05017. https://doi.org/10.1029/2005gc001045
- Syracuse, E. M., van Keken, P. E., & Abers, G. A. (2010). The global range of subduction zone thermal models. *Physics of the Earth and Planetary Interiors*, 183(1–2), 73–90. https://doi.org/10.1016/j.pepi.2010.02.004
- Tian, D. (2023). PyGMT: A Python interface for the generic mapping tools. Zenodo. https://doi.org/10.5281/zenodo.8303186
- Tibi, R., Wiens, D. A., & Yuan, X. (2008). Seismic evidence for widespread serpentinized forearc mantle along the Mariana convergence margin. Geophysical Research Letters, 35(13), L13303. https://doi.org/10.1029/2008g1034163
- Till, C. B., Grove, T. L., & Withers, A. C. (2012). The beginnings of hydrous mantle wedge melting. Contributions to Mineralogy and Petrology, 163(4), 669–688. https://doi.org/10.1007/s00410-011-0692-6
- Tozer, B., Stern, T. A., Lamb, S. L., & Henrys, S. A. (2017). Crust and upper-mantle structure of Wanganui Basin and southern Hikurangi margin, North Island, New Zealand as revealed by active source seismic data. *Geophysical Journal International*, 211(2), 718–740. https://doi.org/10.1093/gji/ggx303

EPSTEIN ET AL. 25 of 27

com/doi/10.1029/2023 AV 001121 by University

- Ulmer, P., & Trommsdorff, V. (1995). Serpentine stability to mantle depths and subduction-related magmatism. *Science*, 268(5212), 858–861. https://doi.org/10.1126/science.268.5212.858
- van Keken, P. E., Hacker, B. R., Syracuse, E. M., & Abers, G. A. (2011). Subduction factory: 4. Depth-dependent flux of H2O from subducting slabs worldwide. *Journal of Geophysical Research*, 116(B1), B01401. https://doi.org/10.1029/2010jb007922
- van Keken, P. E., Kiefer, B., & Peacock, S. M. (2002). High-resolution models of subduction zones: Implications for mineral dehydration reactions and the transport of water into the deep mantle. *Geochemistry, Geophysics, Geosystems*, 3(10), 1. https://doi.org/10.1029/2001gc000256
- Wada, I., Behn, M. D., & Shaw, A. M. (2012). Effects of heterogeneous hydration in the incoming plate, slab rehydration, and mantle wedge hydration on slab-derived H₂O flux in subduction zones. *Earth and Planetary Science Letters*, 353, 60–71. https://doi.org/10.1016/j.epsl.2012.07.025
- Wada, I., & Wang, K. (2009). Common depth of slab-mantle decoupling: Reconciling diversity and uniformity of subduction zones. Geochemistry, Geophysics, Geosystems, 10(10), Q10009. https://doi.org/10.1029/2009gc002570
- Wada, I., Wang, K., He, J., & Hyndman, R. D. (2008). Weakening of the subduction interface and its effects on surface heat flow, slab dehydration, and mantle wedge serpentinization. *Journal of Geophysical Research*, 113(B4), B04402. https://doi.org/10.1029/2007jb005190
- Wang, K., Huang, T., Tilmann, F., Peacock, S. M., & Lange, D. (2020). Role of Serpentinized mantle wedge in affecting Megathrust Seismogenic behavior in the area of the 2010 M = 8.8 Maule earthquake. *Geophysical Research Letters*, 47(22), e2020GL090482. https://doi.org/10.1029/2020gl090482
- Wang, K., Hyndman, R. D., & Yamano, M. (1995). Thermal regime of the southwest Japan subduction zone: Effects of age history of the subducting plate. *Tectonophysics*, 248(1–2), 53–69. https://doi.org/10.1016/0040-1951(95)00028-1
- Wang, Y., Wang, K., He, J., & Zhang, L. (2023). On unusual conditions for the exhumation of subducted oceanic crustal rocks: How to make rocks hotter than models. Earth and Planetary Science Letters, 615, 118213. https://doi.org/10.1016/j.epsl.2023.118213
- Wessel, P., Luis, J. F., Uieda, L., Scharroo, R., Wobbe, F., Smith, W. H., & Tian, D. (2019). The generic mapping tools version 6. Geochemistry, Geophysics, Geosystems, 20(11), 5556–5564. https://doi.org/10.1029/2019gc008515
- Wilson, C. R., Spiegelman, M., van Keken, P. E., & Hacker, B. R. (2014). Fluid flow in subduction zones: The role of solid rheology and compaction pressure. Earth and Planetary Science Letters, 401, 261–274. https://doi.org/10.1016/j.epsl.2014.05.052
- Worzewski, T., Jegen, M., Kopp, H., Brasse, H., & Taylor Castillo, W. (2011). Magnetotelluric image of the fluid cycle in the Costa Rican subduction zone. *Nature Geoscience*, 4(2), 108–111. https://doi.org/10.1038/ngeo1041
- Wunder, B., & Schreyer, W. (1997). Antigorite: High-pressure stability in the system MgO-SiO₂-H₂O (MSH). *Lithos*, 41(1–3), 213–227. https://doi.org/10.1016/s0024-4937(97)82013-0
- Zhong, S., & Gurnis, M. (1995). Mantle convection with plates and mobile, faulted plate margins. Science, 267(5199), 838–843. https://doi.org/10.1126/science.267.5199.838
- Zhong, X., & Galvez, M. E. (2022). The subducting slab as a chromatographic column: Regimes of sub-solidus mass transport as a function of lithospheric hydration state, with special reference to the fate of carbonate. *Journal of Geophysical Research: Solid Earth*, 127(6), e2021JB023851. https://doi.org/10.1029/2021jb023851
- Zhou, X., & Wada, I. (2021). Differentiating induced versus spontaneous subduction initiation using thermomechanical models and metamorphic soles. Nature Communications, 12(1), 4632. https://doi.org/10.1038/s41467-021-24896-x

References From the Supporting Information

- Abe, Y., Ohkura, T., Hirahara, K., & Shibutani, T. (2011). Water transportation through the Philippine Sea slab subducting beneath the central Kyushu region, Japan, as derived from receiver function analyses. *Geophysical Research Letters*, 38(23), L23305. https://doi.org/10.1029/2011gl049688
- Auzanneau, E., Schmidt, M. W., Vielzeuf, D., & Connolly, J. A. (2010). Titanium in phengite: A geobarometer for high temperature eclogites. Contributions to Mineralogy and Petrology, 159, 1–24. https://doi.org/10.1007/s00410-009-0412-7
- Bohm, M., Lüth, S., Echtler, H., Asch, G., Bataille, K., Bruhn, C., et al. (2002). The southern Andes between 36 and 40 S latitude: Seismicity and average seismic velocities. *Tectonophysics*, 356(4), 275–289. https://doi.org/10.1016/s0040-1951(02)00399-2
- Brasse, H., Kapinos, G., Mütschard, L., Alvarado, G. E., Worzewski, T., & Jegen, M. (2009). Deep electrical resistivity structure of northwestern Costa Rica. *Geophysical Research Letters*, 36(2), L02310. https://doi.org/10.1029/2008gl036397
- Brocher, T. M., Parsons, T., Tréhu, A. M., Snelson, C. M., & Fisher, M. A. (2003). Seismic evidence for widespread serpentinized forearc upper mantle along the Cascadia margin. *Geology*, 31(3), 267–270. https://doi.org/10.1130/0091-7613(2003)031<0267:sefwsf>2.0.co;2
- Chou, H. C., Kuo, B. Y., Chiao, L. Y., Zhao, D., & Hung, S. H. (2009). Tomography of the westernmost Ryukyu subduction zone and the serpentinization of the fore-arc mantle. *Journal of Geophysical Research*, 114(B12), B12301. https://doi.org/10.1029/2008jb006192
- Coggon, R., & Holland, T. J. B. (2002). Mixing properties of phengitic micas and revised garnet-phengite thermobarometers. *Journal of Metamorph Geology*, 20(7), 683–696.
- Collings, R., Lange, D., Rietbrock, A., Tilmann, F., Natawidjaja, D., Suwargadi, B., et al. (2012). Structure and seismogenic properties of the Mentawai segment of the Sumatra subduction zone revealed by local earthquake traveltime tomography. *Journal of Geophysical Research*, 117(B1), B01405. https://doi.org/10.1029/2011jb008469
- Contreras-Reyes, E., Grevemeyer, I., Watts, A. B., Flueh, E. R., Peirce, C., Moeller, S., & Papenberg, C. (2011). Deep seismic structure of the Tonga subduction zone: Implications for mantle hydration, tectonic erosion, and arc magmatism. *Journal of Geophysical Research*, 116(B10), B10103. https://doi.org/10.1029/2011jb008434
- Dinc, A. N., Rabbel, W., Flueh, E. R., & Taylor, W. (2011). Mantle wedge hydration in Nicaragua from local earthquake tomography. Geophysical Journal International, 186(1), 99–112. https://doi.org/10.1111/j.1365-246x.2011.05041.x
- Doo, W. B., Lo, C. L., Kuo-Chen, H., Brown, D., & Hsu, S. K. (2015). Exhumation of serpentinized peridotite in the northern Manila subduction zone inferred from forward gravity modeling. *Geophysical Research Letters*, 42(19), 7977–7982. https://doi.org/10.1002/2015gl065705
- Gailler, L., Arcay, D., Münch, P., Martelet, G., Thinon, I., & Lebrun, J. F. (2017). Forearc structure in the Lesser Antilles inferred from depth to the Curie temperature and thermo-mechanical simulations. *Tectonophysics*, 706, 71–90. https://doi.org/10.1016/j.tecto.2017.03.014
- Green, E. C. R., Holland, T. J. B., & Powell, R. (2007). An order-disorder model for omphacitic pyroxenes in the system jadeite-diopside-hedenbergite-acmite, with applications to eclogitic rocks. *American Mineralogist*, 92, 1181–1189.
- Green, E. C. R., White, R. W., Diener, J. F. A., Powell, R., Holland, T. J. B., & Palin, R. M. (2016). Activity-composition relations for the calculation of partial melting equilibria in metabasic rocks. *Journal of Metamorphic Geology*, 34(9), 845–869. https://doi.org/10.1111/jmg. 12211

EPSTEIN ET AL. 26 of 27

om/doi/10.1029/2023AV001121 by University Of Miami Libraries

and-conditions) on Wiley Online Library for rules

are governed by the applicable Creativ

- Grevemeyer, I., & Tiwari, V. M. (2006). Overriding plate controls spatial distribution of megathrust earthquakes in the Sunda–Andaman subduction zone. Earth and Planetary Science Letters, 251(3–4), 199–208. https://doi.org/10.1016/j.epsl.2006.08.021
- Husen, S., Quintero, R., Kissling, E., & Hacker, B. (2003). Subduction-zone structure and magmatic processes beneath Costa Rica constrained by local earthquake tomography and petrological modelling. *Geophysical Journal International*, 155(1), 11–32. https://doi.org/10.1046/j.1365-246x.2003.01984.x
- Kamimura, A., Kasahara, J., Shinohara, M., Hino, R., Shiobara, H., Fujie, G., & Kanazawa, T. (2002). Crustal structure study at the Izu-Bonin subduction zone around 31 N: Implications of serpentinized materials along the subduction plate boundary. *Physics of the Earth and Planetary Interiors*, 132(1–3), 105–129. https://doi.org/10.1016/s0031-9201(02)00047-x
- Kamiya, S. I., & Kobayashi, Y. (2000). Seismological evidence for the existence of serpentinized wedge mantle. Geophysical Research Letters, 27(6), 819–822. https://doi.org/10.1029/1999gl011080
- Krawczyk, C. M., Mechie, J., Lüth, S., Tašárová, Z., Wigger, P., Stiller, M., et al. (2006). Geophysical signatures and active tectonics at the south-central Chilean margin. Andes: Active Subduction Orogeny, 171–192. https://doi.org/10.1007/978-3-540-48684-8_8
- Matsubara, M., Hayashi, H., Obara, K., & Kasahara, K. (2005). Low-velocity oceanic crust at the top of the Philippine Sea and Pacific plates beneath the Kanto region, central Japan, imaged by seismic tomography. *Journal of Geophysical Research*, 110(B12). https://doi.org/10.1029/2005jb003673
- Matsubara, M., Obara, K., & Kasahara, K. (2009). High-VP/VS zone accompanying non-volcanic tremors and slow-slip events beneath southwestern Japan. *Tectonophysics*, 472(1–4), 6–17. https://doi.org/10.1016/j.tecto.2008.06.013
- Planert, L., Kopp, H., Lueschen, E., Mueller, C., Flueh, E. R., Shulgin, A., et al. (2010). Lower plate structure and upper plate deformational segmentation at the Sunda-Banda arc transition, Indonesia. *Journal of Geophysical Research*, 115(B8), B12304. https://doi.org/10.1029/2009jb006713
- Soyer, W., & Unsworth, M. (2006). Deep electrical structure of the northern Cascadia (British Columbia, Canada) subduction zone: Implications for the distribution of fluids. *Geology*, 34(1), 53–56. https://doi.org/10.1130/g21951.1
- Tajčmanová, L., Connolly, J. A. D., & Cesare, B. (2009). A thermodynamic model for titanium and ferric iron solution in biotite. *Journal of metamorphic geology*, 27(2), 153–165. https://doi.org/10.1111/j.1525-1314.2009.00812.x
- Uchida, N., Nakajima, J., Hasegawa, A., & Matsuzawa, T. (2009). What controls interplate coupling? Evidence for abrupt change in coupling across a border between two overlying plates in the NE Japan subduction zone. *Earth and Planetary Science Letters*, 283(1–4), 111–121. https://doi.org/10.1016/j.epsl.2009.04.003
- Xia, S., Sun, J., & Huang, H. (2015). Degree of serpentinization in the forearc mantle wedge of Kyushu subduction zone: Quantitative evaluations from seismic velocity. *Marine Geophysical Researches*, 36(2–3), 101–112. https://doi.org/10.1007/s11001-014-9239-3
- Xia, S., Zhao, D., & Qiu, X. (2008). Tomographic evidence for the subducting oceanic crust and forearc mantle serpentinization under Kyushu, Japan. *Tectonophysics*, 449(1–4), 85–96. https://doi.org/10.1016/j.tecto.2007.12.007
- White, R. W., Powell, R., Holland, T. J. B., Johnson, T. E., & Green, E. C. R. (2014). New mineral activity-composition relations for thermodynamic calculations in metapelitic systems. *Journal of Metamorphic Geology*, 31, 261–286. https://doi.org/10.1111/jmg.12071
- Whitney, D. L., & Evans, B. W. (2010). Abbreviations for names of rock-forming minerals. American Mineralogist, 95(1), 185–187. https://doi.org/10.2138/am.2010.3371

EPSTEIN ET AL. 27 of 27